Review

2D Bi$_2$Se$_3$ materials for optoelectronics

Fakun K. Wang,[1] Sijie J. Yang,[1] and Tianyou Y. Zhai[1,*]

SUMMARY

2D layered materials with diverse exciting properties have recently attracted tremendous interest in the scientific community. Layered topological insulator Bi$_2$Se$_3$ comes into the spotlight as an exotic state of quantum matter with insulating bulk states and metallic Dirac-like surface states. Its unique crystal and electronic structure offer attractive features such as broadband optical absorption, thickness-dependent surface bandgap and polarization-sensitive photoresponse, which enable 2D Bi$_2$Se$_3$ to be a promising candidate for optoelectronic applications. Herein, we present a comprehensive summary on the recent advances of 2D Bi$_2$Se$_3$ materials. The structure and inherent properties of Bi$_2$Se$_3$ are firstly described and its preparation approaches (i.e., solution synthesis and van der Waals epitaxy growth) are then introduced. Moreover, the optoelectronic applications of 2D Bi$_2$Se$_3$ materials in visible-infrared detection, terahertz detection, and opto-spintronic device are discussed in detail. Finally, the challenges and prospects in this field are expounded on the basis of current development.

INTRODUCTION

Two-dimensional (2D) layered materials hold great promise for the technological advancement of next-generation electronic and optoelectronic devices. Compared with their bulk counterparts, 2D layered materials usually show unique features because of quantum confinement effect along the vertical direction of the 2D plane (Akinwande et al., 2014; Liu et al., 2020a, 2020b, 2020c; Ricciardulli et al., 2021). Atomically smooth surfaces without dangling bonds enable them to be compatible with any 2D materials and mature complementary metal oxide semiconductor (CMOS) process without considering lattice matching (Akinwande et al., 2019; Iannaccone et al., 2018; Liang et al., 2019; Liu et al., 2019a, 2019b; Wang et al., 2021a, 2021b, 2021c, 2021d). Moreover, the electronic band structures of 2D layered materials cover a wide range of electromagnetic spectrum, meaning that diverse optical and electrical properties reside in their family (Liu et al., 2021a, 2021b; Xia et al., 2014). In the last decade, a wealth of 2D layered materials have been isolated from bulk crystals or been fabricated through bottom-up synthesis (Cai et al., 2018; Fang et al., 2021; Han et al., 2019a, 2019b; Li et al., 2017; Varoon et al., 2011; Wang et al., 2020a, 2020b; Zhou et al., 2018). Their fundamental physical properties and demonstrative functional devices have been thoroughly studied (Koppens et al., 2014; Sierra et al., 2021; Wang et al., 2019a, 2019b, 2019c, 2021a, 2021b, 2021c, 2021d)). These thereby vastly promote the application of 2D layered materials in next-generation advanced devices.

Among numerous 2D layered materials, topological insulator Bi$_2$Se$_3$ as an unusual phase of quantum matter has attracted tremendous research interest in the scientific community. Insulating bulk states with a band energy gap of ∼0.3 eV and conducting gapless surface states consisting of a single Dirac cone co-exist in a thin layer of Bi$_2$Se$_3$, which has been verified theoretically and experimentally (He et al., 2010; Kim et al., 2012; Peng et al., 2010; Zhang et al., 2009). Topological surface states protected by time inversion symmetry possess spin-momentum locking helical nature, which can suppress electron backscattering and enable excellent carrier mobility (∼10^3 cm^2 V^{-1} s^{-1}) (Bansal et al., 2012; Bhattacharyya et al., 2017a, 2017b; He et al., 2012; Steinberg et al., 2010). In addition, Bi$_2$Se$_3$ demonstrates attractive optoelectronic properties such as broadband optical absorption (Guo et al., 2013; Peng et al., 2012; Yao et al., 2014), thickness-dependent surface bandgap (He et al., 2010; Post et al., 2013) and polarization-sensitive photocurrent (Besbas et al., 2016; Duan et al., 2014; Yan et al., 2014). These intriguing properties are favorable for Bi$_2$Se$_3$ as a promising candidate for optoelectronic devices (Bhattacharyya et al., 2018a, 2018b; Sharma et al., 2016; Wang et al., 2019a, 2019b, 2019c; Zhang et al., 2010). Up to now, a large amount of efforts have been devoted and significant progress have been made in the study of 2D Bi$_2$Se$_3$ from materials preparation to optoelectronic applications.

[1]State Key Laboratory of Materials Processing and Die & Mould Technology, School of Materials Science and Engineering, Huazhong University of Science and Technology, Wuhan 430074, P. R. China

*Correspondence: zhaity@hust.edu.cn
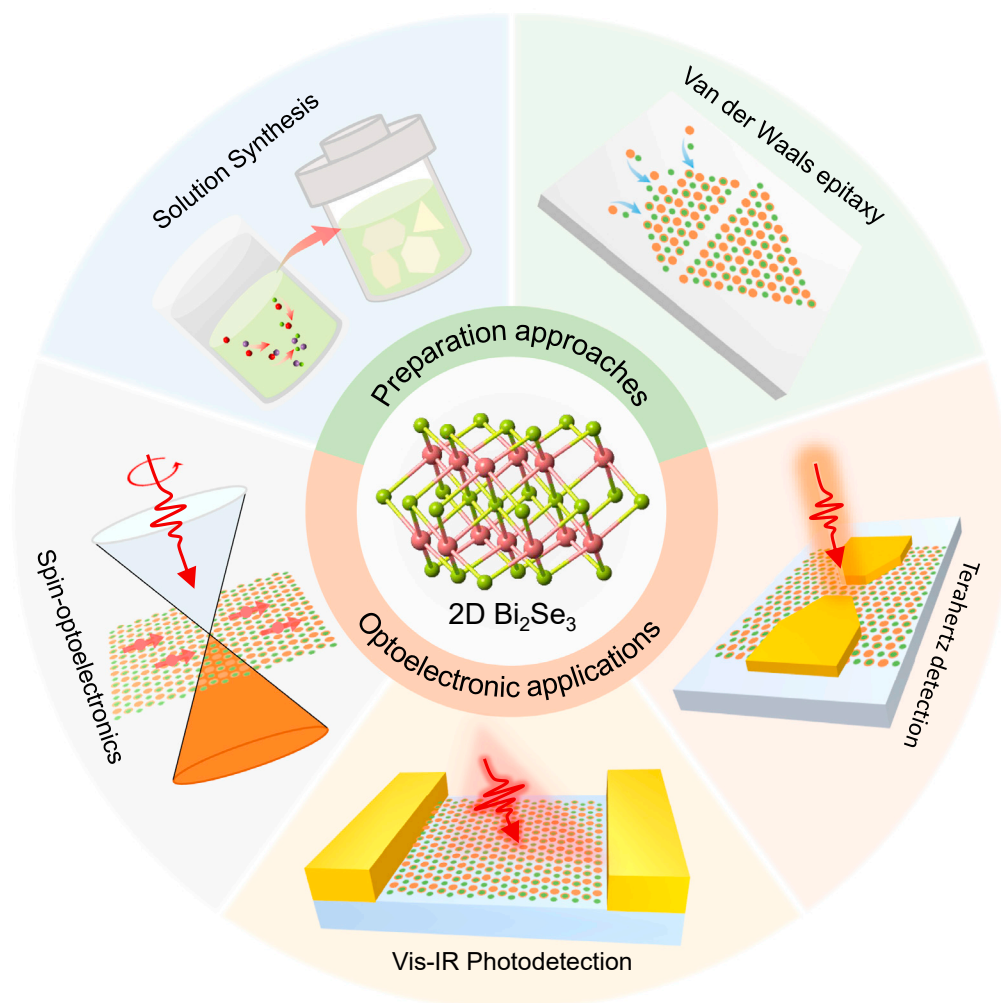
Figure 1. Schematic illustration of preparation approaches and optoelectronic applications of 2D Bi$_2$Se$_3$ materials

To promote the further development of 2D Bi$_2$Se$_3$ research and technology, it is necessary to make a comprehensive summary and reasonable outlook. Inspired by this, we provide an overview in terms of the recent advances (Figure 1). The structure and properties of 2D Bi$_2$Se$_3$ are firstly introduced. Subsequently, the preparation approaches of 2D Bi$_2$Se$_3$ are summarized in detail, including solution synthesis and van der Waals epitaxy growth. We then emphasize the optoelectronic applications of 2D Bi$_2$Se$_3$ in visible-infrared detection, terahertz detection, and opto-spintronic device. Lastly, several insights are given into the technical challenges and potential solutions towards future development of 2D Bi$_2$Se$_3$-based optoelectronics.

STRUCTURE AND PROPERTY OF 2D BI$_2$SE$_3$ MATERIAL

The crystal structure of Bi$_2$Se$_3$ is rhombohedral with space group D_{3d}^5 (*R*-3m). Viewed along the *z*-direction (Figure 2A), the Bi$_2$Se$_3$ crystal can be regarded as a layered compound formed by periodic stacking of quintuple layers (QL) with the sequence -A(Se1)-B(Bi1)-C(Se2)-B(Bi1')-A(Se1'), where 1 and 2 refer to two different chemical states for the Se anions. In one QL, the Se2 anions in the middle are almost octahedral in coordination with six adjacent Bi1 cations, whereas the outermost Se1 anions are strongly bound to three Bi1 cations in the same layer. Se1 anions in two adjacent QLs are coupled by van der Waals force, indicating that the Bi$_2$Se$_3$ crystal is easy to cleave between adjacent Se1 layers. In addition, the Se1 (Bi1) layer can be changed to the Se1' (Bi1') layer by an inversion operation with the Se2 layer as the inversion center. From the top view along the *z*-direction, there are three different sites in the triangle lattice in a QL, namely A, B,
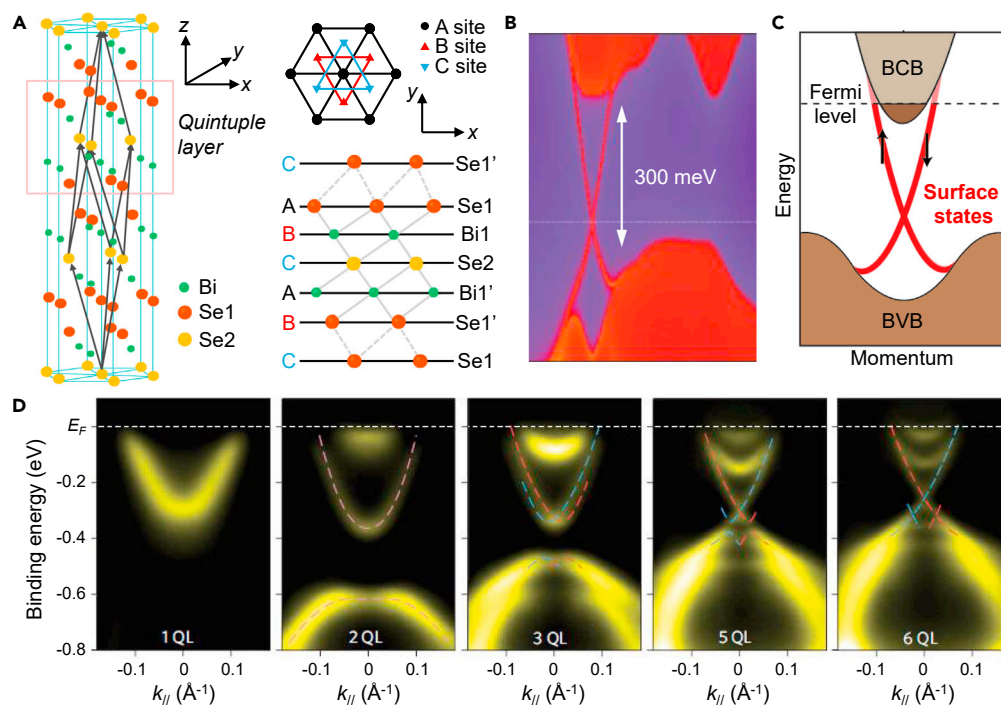
Figure 2. Crystal structure and physical properties of Bi$_2$Se$_3$

(A) The schematic of layered crystal structure of Bi$_2$Se$_3$.

(B) Theoretically calculated electronic band structure of Bi$_2$Se$_3$ with a bulk energy gap of 0.3 eV and gapless lines dispersing. (A and B) Reproduced with permission from (Zhang et al., 2009). Copyright 2009 Springer Nature.

(C) Schematic of the band structure of Bi$_2$Se$_3$, depicting the spin-momentum locking surface states. The up and down arrow represent spin-up and spin-down, respectively. Reproduced with permission from (Hsieh et al., 2009). Copyright 2009 Macmillan Publishers Limited.

(D) ARPES spectra of 1-6QLs Bi$_2$Se$_3$, showing that the surface states do not exist in Bi$_2$Se$_3$ with less than 6QLs. Reproduced with permission from (He et al., 2010). Copyright 2010 Springer Nature.

and C, indicating the three-fold rotation symmetry of Bi$_2$Se$_3$ crystal. The lattice constants of Bi$_2$Se$_3$ are $a = b = 4.140$ Å and $c = 28.636$ Å and each unit cell spans over 3 QLs. Therefore, the thickness of each QL (monolayer Bi$_2$Se$_3$) is ∼9.55 Å.

Bi$_2$Se$_3$ has a very unique electronic band structure, thus exhibiting many novel physical properties. In 2009, Zhang et al. performed comprehensive theoretical calculations on the electronic energy band structure of Bi$_2$Se$_3$ by considering the effect of crystal-field splitting and spin-orbit coupling on the energy eigenvalues (Zhang et al., 2009). Their calculation results predict that Bi$_2$Se$_3$ is a topological insulator with insulating bulk states and conducting topological surface states. As shown in Figure 2B, a topologically non-trivial energy gap of 0.3 eV and a single Dirac cone could be observed from the energy and momentum dependence of the local density of states at Γ point (Zhang et al., 2009). The electrons on the topological surface states possess a spin-momentum-locked relationship (Figure 2C) that is protected by time-reversal symmetry, enabling them to avoid interference from non-magnetic impurities (Hsieh et al., 2009). In the meanwhile, experimental studies using angle-resolved photoemission spectroscopy (ARPES) and scanning tunneling microscopy have provided the visual topological surface states of Bi$_2$Se$_3$ (Bianchi et al., 2010; Zhang et al., 2013), which is similar to the dispersion relationship predicted by Zhang et al. (Zhang et al., 2009). Since then, a great deal of theoretical calculations and experimental researches have been devoted to the study of topological insulators, and many novel physical properties have been revealed (Dankert et al., 2015; Kim et al., 2012, 2014; Kong and Cui, 2011; Liu et al., 2014; Luo et al., 2019; Sacepe et al., 2011). One of the important properties is that the topological surface states are strongly dependent on the thickness of Bi$_2$Se$_3$. As presented in Figure 2D, the ARPES spectra of Bi$_2$Se$_3$ thin films grown by molecular beam epitaxy (MBE) demonstrate the thickness-dependent band maps, in which the Dirac cone opening is clearly observed when the thickness is thinner than 6 QLs (He et al., 2010). Moreover, the opened

topological surface states exhibited sizable Rashba splitting due to the surface potential difference induced by the substrate. In addition, Wang et al. directly observed the surface-dominated conduction in a 6 QLs Bi_2Se_3 thin film through the Hall effect test (He et al., 2012). These research results indicate that the Bi_2Se_3 with thickness above 6 QLs is topologically non-trivial while it is topologically trivial as thickness below 6 QLs.

The unique electronic band structure brings novel electrical properties to Bi_2Se_3. For example, the conductance of Bi_2Se_3 was thought to be contributed by both its topological surface states and bulk states. Pablo et al. evaluated the different contribution of topological surface states and bulk states of a 17 QLs Bi_2Se_3 flake through transport measurements (Steinberg et al., 2010). The as-evaluated carrier concentration of bulk states and topological surface states were about 1×10^{19} cm^{-2} and 4×10^{13} cm^{-2}, and the mobility of ones were 1700 cm V^{-1} s^{-1} and 1000 cm V^{-1} s^{-1}, respectively. Besides, Seongshik et al. found that the carrier concentration and mobility of Bi_2Se_3 demonstrated independence on the thickness in the range of 8–256 QLs by performing thickness-dependent transport measurements at a temperature of 1.5 K, which remained around 1×10^{13} cm^{-2} and 2×10^3 cm V^{-1} s^{-1}, respectively (Bansal et al., 2012). Although the carrier concentration and mobility decreased as the thickness decreased when the thickness was in the range of 2–8 QLs. The reason for this change was that the lack of topological surface states in the thin sample reduced their contribution to the conductance (Bansal et al., 2012). Generally, the coexistence of bulk states and topological surface states opens new possibilities for novel electronic and optoelectronic devices. It should be noted that the research on the topological surface states of Bi_2Se_3 usually requires an extremely low temperature environment, because thermal perturbations tend to excite narrow-bandgap bulk states and thus annihilate the physical properties of topological surface states.

PREPARATION OF 2D Bi_2Se_3 MATERIALS

Preparing 2D Bi_2Se_3 materials is of great significance for studying novel properties and exploiting functional devices. Compared with the bulk counterpart, 2D Bi_2Se_3 possesses a larger surface-to-volume ratio and more tailorability, in favor of investigating topological surface states and regulating physical properties. Currently, the approaches widely used to prepare 2D Bi_2Se_3 materials include mechanical exfoliation, molecular beam epitaxy, solution synthesis and van der Waals epitaxial growth (Guo et al., 2015; Kong and Cui, 2011). Mechanical exfoliation is a process in which the bulk Bi_2Se_3 crystals are cleaved into 2D nanosheets by artificial mechanical forces stronger than interlayer van der Waals interactions. The high crystallinity of bulk crystals can be inherited to the as-exfoliated 2D nanosheets, which is advantageous for investigating their intrinsic physical properties. However, the serious challenge faced by the mechanical exfoliation is that the morphology, thickness and yield of samples are uncontrollable (Cho et al., 2011; Hong et al., 2010). The high quality 2D Bi_2Se_3 single crystal films with controllable thickness could be produced by molecular beam epitaxy, but the experimental equipment is expensive and less accessible, which is difficult for industrial production (Chen et al., 2011). Fortunately, solution synthesis and van der Waals epitaxy growth have demonstrated promising prospects in scalable production of 2D Bi_2Se_3 materials. In this section, we will focus on the two production approaches for 2D Bi_2Se_3 materials.

Solution synthesis

Solution synthesis has been widely used in the laboratory to prepare 2D materials. This approach involves chemical reaction processes in which one or more reactants are converted to one or more different products by rearranging constituent atoms. The reactions usually take place in an autoclave containing water or organic solutions (Figure 3A). Under suitable conditions, these reactants react with each other after reaching the chemical reaction activity, and finally produce the desired products. Importantly, the morphology, size, thickness, and crystallinity of the products can be precisely controlled by changing the reactant, solvent, reaction temperature and time (Liu et al., 2019a, 2019b; Zhuang et al., 2014). For example, Xiong et al. obtained 2D Bi_2Se_3 crystals by using $Bi(NO_3)_3 \cdot 5H_2O$ and Na_2SeO_3 as reactants in a mixed solution of poly(vinylpyrrolidone) and ethylene glycol (Zhang et al., 2011). As shown in Figure 3B, the as-synthesized 2D Bi_2Se_3 crystals presented a hexagonal shape with a lateral size of micrometers. The clear and bright selected-area electron diffraction pattern presented in Figure 3C demonstrated the high crystallinity of 2D Bi_2Se_3 crystals synthesized by this approach (Zhang et al., 2011). Their study focused on the Raman optics of 2D Bi_2Se_3 crystals, but the growth mechanism was not revealed.

Subsequently, Jeong et al. performed detailed studies on the growth mechanism of 2D Bi_2Se_3 crystals synthesized in solutions (Min et al., 2012). In their studies, the reaction sources and organic solvents
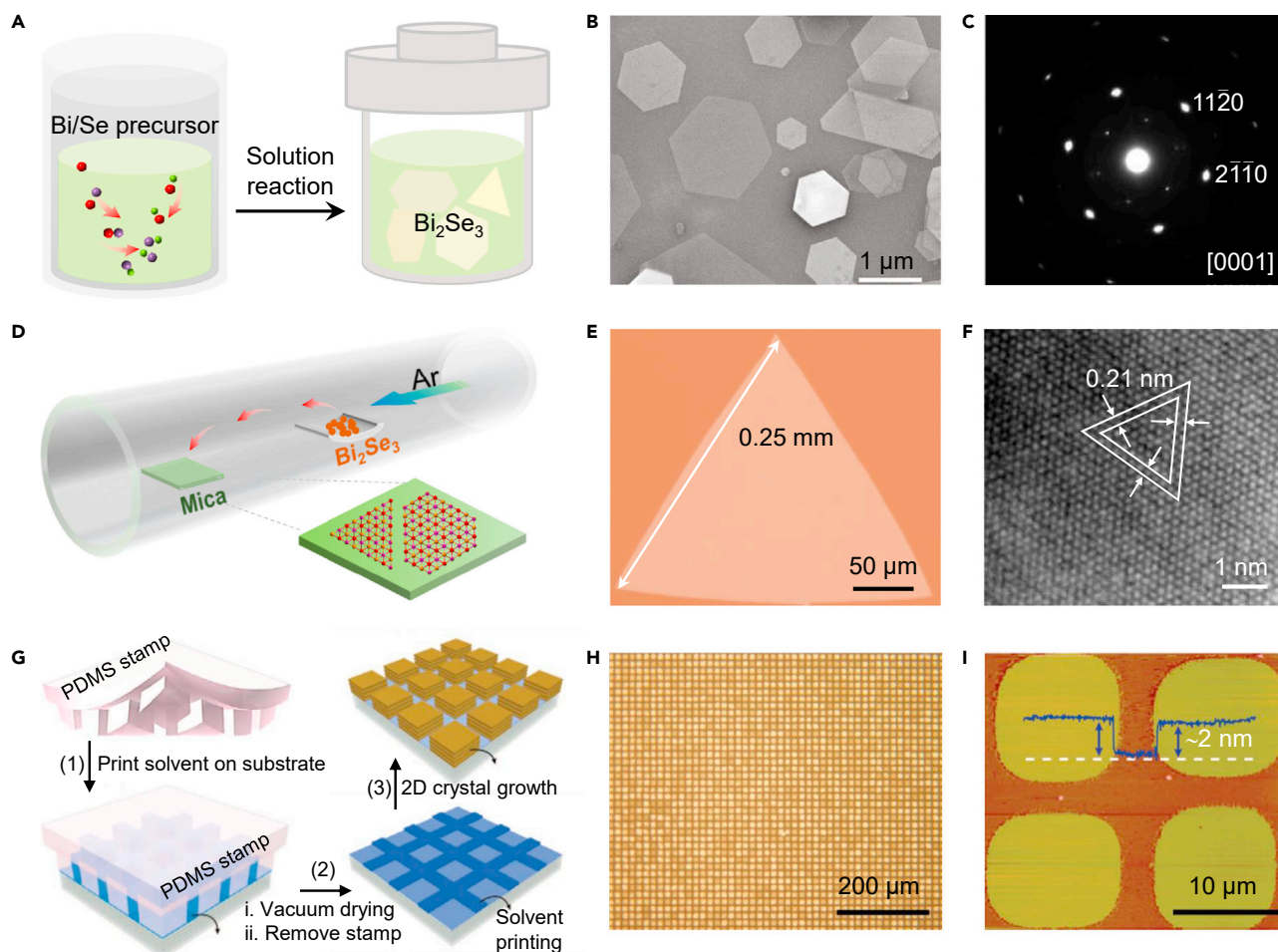
Figure 3. Preparation approaches of 2D Bi₂Se₃ flakes

(A) Schematic diagram of solution synthesis of Bi₂Se₃ flakes.

(B) Morphology of the as-synthesized Bi₂Se₃ flakes.

(C) Selected area diffraction pattern of Bi₂Se₃ flakes. (B and C) Reproduced with permission from (Zhang et al., 2011). Copyright 2011 American Chemical Society.

(D) Schematic illustration of van der Waals epitaxial growth of Bi₂Se₃ flakes.

(E) Optical image of a triangular Bi₂Se₃ flake with a lateral size of 0.25 mm.

(F) High-magnification TEM image of the as-grown Bi₂Se₃ flake. (D–F) Reproduced with permission from (Wang et al., 2018). Copyright 2018 WILEY-VCH Verlag GmbH & Co. KGaA, Weinheim.

(G) Schematic representation of procedures for patterning of 2D Bi₂Se₃ flakes.

(H) Representative optical image of large-scale Bi₂Se₃ array.

(I) Atomic force microtopography of a 2 × 2 Bi₂Se₃ array with a uniform thickness of 2 nm. (G-I) Reproduced with permission from (Zheng et al., 2015). Copyright 2015 Springer Nature.

used were the same as those used by Xiong et al., but the reducing agent hydroxylamine was added to speed up the chemical reaction. They found that small Bi₂Se₃ crystals were nucleated within 5 s and then grew into larger crystals after rapid injection of the reducing agent hydroxylamine into the reaction solutions at 180°C and the reaction temperature quickly dropped to 160°C. When the temperature was restored to 180°C, additional generated small crystals would adsorb to the surface of previous crystals and further recrystallize to form the second Bi₂Se₃ layer. Moreover, the authors believed that the negatively charged Se atomic layer in Bi₂Se₃ was the internal driving force for the adsorption and recrystallization of crystals, and added positively charged surfactants poly(ethylene imine) into the solution to hinder the growth of 2D Bi₂Se₃ crystals along the z-axis (Min et al., 2012). The discovery of this growth mechanism provides important guidance for the subsequent preparation of 2D Bi₂Se₃ materials by solution synthesis.

Recently, Pradhan et al. have successfully obtained single-crystalline 2D Bi_2Se_3 nanosheets using colloidal synthesis method by hot injection of bismuth-complex precursor to selenium complex precursor (Pradhan et al., 2020). In this method, the bismuth-complex precursor was prepared by dissolving bismuth acetate $(Bi(OAc)_3)$ in a mixture of short-chain octylamine (OctAm) and octanoic acid (OctAc) ligands along with oleic acid (OLAc) at 100°C, and the selenium complex precursor was prepared by virtue of four ligands (Oleylamine (OLAm), OctAm, OctAc, OLAc) and non-coordinating solvent octadecene to dissolve Se powder at 180°C. These short-chain of amine and acid as well as relatively low reaction temperature promoted the expansion of the lateral dimension of 2D Bi_2Se_3 nanosheets, resulting in a size of several microns. The growth mechanism of the 2D Bi_2Se_3 nanosheets was considered to be oriented attachment, that is, the small Bi_2Se_3 nanocrystals first undergo oriented attachment and then epitaxially recrystallized (Pradhan et al., 2020). This colloidal synthesis method with oriented attachment growth mechanism has also been used to fabricate metal (Sb, Mn, Cu)-doped or intercalated 2D Bi_2Se_3 nanosheets, which enrich the physical properties of 2D Bi_2Se_3 materials (Maiti et al., 2021).

Van der Waals epitaxy growth

Van der Waals epitaxy growth is a powerful technique for preparing high-quality 2D materials, without requirement on the lattice matching between the epitaxial layer and substrate (Han et al., 2019a, 2019b; Li et al., 2020a, 2020b). The epitaxial layer interacts with the substrate through weak van der Waals forces rather than chemical bonds, which ensures the epitaxial layer grows into large-size crystals. Bi_2Se_3 has a layered structure with a dangling-bond-free surface and lots of dangling bonds on its edges. This anisotropic bonding property makes the in-plane growth of 2D Bi_2Se_3 nanostructure preferential to the out-of-plane growth (Li et al., 2012). Therefore, the 2D Bi_2Se_3 crystals prepared by van der Waals epitaxial growth possess not only high crystal quality but also large lateral size.

In the van der Waals epitaxy growth of 2D Bi_2Se_3 crystals (Figure 3D), high-purity Bi_2Se_3 powders were usually utilized as the precursor and were evaporated into gaseous sources in a tube furnace (Wang et al., 2018). The as-vaporized gaseous sources were transported to the substrate placed at the downstream of the tube furnace by inert carrier gas, finally nucleating and growing into large-size 2D single crystals. By using this method, Cui et al. obtained atomically thin 2D Bi_2Se_3 flakes with a maximum lateral size of ~20 μm on amorphous SiO_2 substrates (Kong et al., 2010). Although the size is larger than that of crystals prepared by solution synthesis, it is difficult to expand further because the dangling bands on the surface of SiO_2 severely hinder the migration of the precursor on the growth substrates (Zhou et al., 2019). Therefore, the selection of suitable growth substrate is of great importance for the preparation of large-size 2D Bi_2Se_3 crystals. Layered materials such as graphene, h-BN and mica with atomically smooth surfaces were used as the growth substrates of 2D Bi_2Se_3 crystals in subsequent research (Dang et al., 2010; Xu et al., 2015). Among them, the mica substrate has demonstrated more promising potential in the growth of large-size 2D Bi_2Se_3 crystals. For example, Zhai et al. achieved the controllable preparation of submillimeter 2D Bi_2Se_3 crystals on mica substrates by van der Waals epitaxy (Wang et al., 2018). As shown in Figures 3E and 3F, the as-obtained crystal possessed a lateral size of up to 0.25 mm and high crystal quality. Such large lateral sizes could be attributed to the absence of dangling bonds on the mica surface, which greatly facilitated the migration, nucleation and growth of the precursor on the substrate surface (Wang et al., 2018).

The nucleation and growth of Bi_2Se_3 on the mica substrates are random; it is therefore particularly important to realize position-controlled growth for its batch production, fabrication, and integration. For this purpose, a series of methods were developed by Peng and co-authors for the patternable growth of 2D Bi_2Se_3 crystals (Li et al., 2012; Wang et al., 2016; Zheng et al., 2015). The first method was to modify specific regions of the mica surface by using selective oxygen plasma etching, with copper grids or patterned polymethyl methacrylate (PMMA) films as the masks. The morphology and chemical composition of the etched regions could dramatically change, resulting in the inability to epitaxially grow 2D Bi_2Se_3 crystals. Nevertheless, the regions protected by the masks retained the characteristics of epitaxial growth, thereby realizing position-controlled growth of Bi_2Se_3 (Li et al., 2012). The second method was microintaglio printing, as shown in Figure 3G (Zheng et al., 2015). The freshly cleaved mica substrates were first intaglio printed by solvent ink utilizing polydimethylsiloxane (PDMS) stamps with surface relief structures. The solvent ink was then vacuum-dried and PDMS was removed from the mica substrate. The resulting mica modified with intaglio patterns was used for selective-region epitaxy growth of 2D Bi_2Se_3 crystals. Consequently, 2D Bi_2Se_3 crystal arrays with lateral size of ~10 μm and uniform thickness of ~2 nm were achieved by this method (Figures 3H

and 3I) (Zheng et al., 2015). The advantage of this method is that the desired reliefs can be designed on the PDMS to obtain 2D Bi_2Se_3 crystal arrays with different patterns. Analogously, a strategy of selective-region chemical modification of the substrates was proposed by Peng and co-authors for patterned growth of 2D Bi_2Se_3 crystals (Wang et al., 2016). The nucleation energy barrier of 2D Bi_2Se_3 crystals could be modulated by surface engineering of combining micro-contact printing with self-assembly of octadecyltrichlorosilane (OTS) molecules. Specifically, Bi_2Se_3 crystals preferentially crystallized in the chemically modified regions, thereby forming arrayed patterns (Wang et al., 2016). The patterned 2D Bi_2Se_3 crystals exhibit complete array structure, consistent growth orientation and uniform thickness, which is of great significance to batch fabrication and integration of electronic and optoelectronic devices.

The development of simple and convenient growth schemes for attractive 2D Bi_2Se_3 materials is of much interest. For example, Husale and co-workers introduced a one-step confined thin melting approach to prepare 2D nanostructures of topological insulator Bi_2Te_3 (Sharma et al., 2019). In this approach, the top growth substrate was directly in contact with the bottom Bi_2Te_3 thin film precursor deposited by sputtering. The molten species of Bi and Te were formed by heating the precursor and simultaneously diffused onto the growth substrate, in which they got adsorbed and nucleated to produce the nanosheets. Additionally, the Bi_2Te_3 nanostructures could be patterned growth on lithographically patterned substrates in the approach, which provides an important reference for the future development of simple and low-cost methods for the preparation of 2D Bi_2Se_3 and other topological insulator materials.

OPTOELECTRONIC APPLICATIONS OF 2D BI_2SE_3 MATERIALS

In the past few years, 2D Bi_2Se_3 materials have attracted enormous attention from researchers because of its unique physical property as a topological insulator and high carrier mobility as well as a narrow bulk bandgap of ~0.3 eV. The topological surface states of Bi_2Se_3 possess linear Dirac dispersion and helical spin texture, which give rise to fascinating physical phenomena like spin-polarized surface current. The thickness-moderated surface bandgap and occupation of empty surface states can be used to enhance the photo-response of Bi_2Se_3. In addition, the plasmonic excitation of the Dirac fermions arising from topological surface states lies in the tetrahertz range, which makes Bi_2Se_3 responsive to terahertz irradiation. Given these novel physical properties, 2D Bi_2Se_3 is considered to have huge application potential in optoelectronic devices. In this section, we will highlight several typical optoelectronic applications of 2D Bi_2Se_3, including visible-infrared photodetection, terahertz detection and opto-spintronic device.

Visible-infrared photodetection

The visual electronic band structure of 2D Bi_2Se_3 crystal was detected by ARPES measurements in the work of Peng and coauthors (Peng et al., 2012), as shown in Figure 4A. Although the bulk conduction band was partially occupied on account of the electron doping from defects during growth, the 2D Bi_2Se_3 crystal was not completely transparent in the ultraviolet-visible-infrared (UV-Vis-IR) spectrum because there was still a certain transition from the valence band to the occupied state. The optical transmittance of 2D Bi_2Se_3 crystal was negatively correlated with its thickness, and had an average visible transmittance between 60 and 70% in a ~6-nm-thick nanosheet film (Figure 4B), indicating that Bi_2Se_3 absorbed part of the incident light (Peng et al., 2012). Liu et al. demonstrated the near and mid-infrared optical absorption of 2D Bi_2Se_3 crystal with various thicknesses from 5 to 25 nm (Liu et al., 2019a, 2019b). As displayed in Figure 4C, the 2D Bi_2Se_3 crystal exhibited obvious optical absorption in the near and mid-infrared region and the characteristic that the absorbance increases with thickness is similar to other 2D layered materials. This dependence can be explained by the quantum confinement effect (Liu et al., 2019a, 2019b). The wide spectral absorption of Bi_2Se_3 make it a promising candidate material for constructing visible-infrared photodetectors (Hong et al., 2020; Liu et al., 2020a, 2020b, 2020c; Luo et al., 2021a, 2021b; Zhang et al., 2010).

For instance, Zhong et al. reported visible photodetectors based on 2D Bi_2Se_3 nanosheets which were synthesized by hydrothermal intercalation and exfoliation route (Zang et al., 2014). The responsivity and response time of this Bi_2Se_3 nanosheet-based photodetector under 532 nm laser illuminations were determined to be 20.48 mA W^{-1} and 0.7 s, respectively. Zhai et al. demonstrated near-infrared photo-response properties of 2D Bi_2Se_3 flakes grown via van der Waals epitaxy (Wang et al., 2018). As shown in Figures 4D and 4E, the photodetector based on these Bi_2Se_3 flakes presented excellent sensitivity and good reproducibility under the excitation of near-infrared light at the wavelength of 1456 nm, which showed a superior responsivity of 2.74 A W^{-1} and a high detectivity of 3.3 × 10^{10} Jones, but with a slow response time of ~0.5 s at room temperature. These photodetection performance could be further improved to 23.89 A
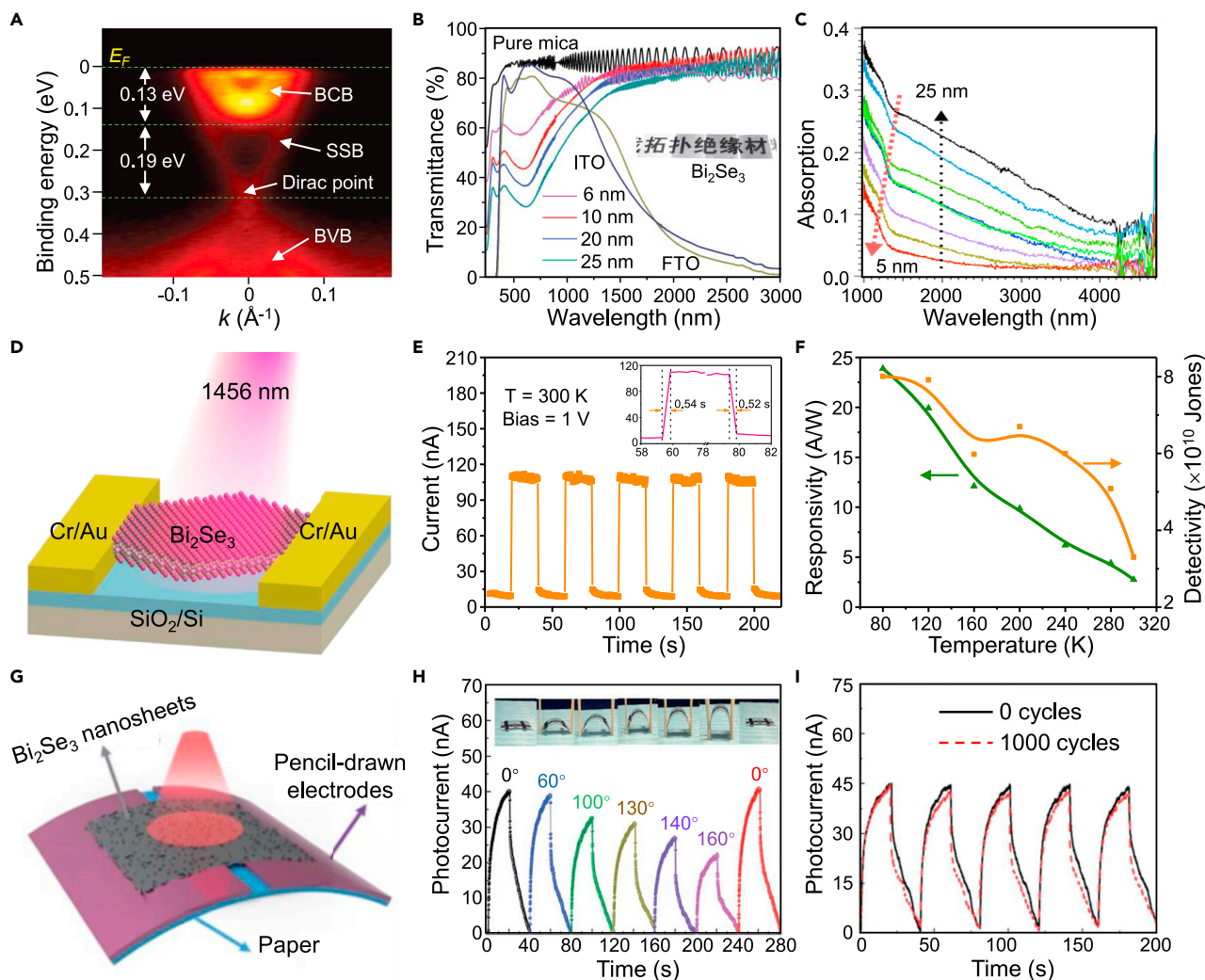
Figure 4. Visible-infrared photodetection of 2D Bi$_2$Se$_3$ flakes

(A) ARPES band dispersion of a 2D Bi$_2$Se$_3$ flake.

(B) UV-vis-IR transmittance spectra of 2D Bi$_2$Se$_3$ flakes with different thicknesses. (A and B) Reproduced with permission from (Peng et al., 2012). Copyright 2012 Springer Nature.

(C) Near and mid-infrared absorption spectra of 2D Bi$_2$Se$_3$ flakes with different thicknesses. Reproduced with permission from (Liu et al., 2019a, 2019b). Copyright 2019 AIP Publishing.

(D) Schematic illustration of a photodetector based on 2D Bi$_2$Se$_3$ flake.

(E) Time-resolved photoresponse of the photodetector under 1456 nm illumination. Inset: the response rate with rising time 0.54 s and decay time 0.52 s.

(F) Temperature-dependent responsivity and detectivity of photodetector. (D-F) Reproduced with permission from (Wang et al., 2018). Copyright 2018 WILEY-VCH Verlag GmbH & Co. KGaA, Weinheim.

(G) Schematic diagram of a flexible photodetector based on Bi$_2$Se$_3$ nanosheets with pencil-drawn graphite as the electrodes and paper as the substrate.

(H) Time-resolved photoresponse of the flexible photodetector under different bending angles.

(I) Time-photocurrent curves of the flexible photodetector after bending 0 cycles and 1000 cycles. (G–I) Reproduced with permission from (Liu et al., 2020a, 2020b, 2020c). Copyright 2020 Royal Society of Chemistry.

W^{-1} and 8.0 × 10^{10} Jones when the operating temperature of the device was reduced to 80 K (Figure 4F), which were attributed to weaker Coulomb scattering and phonon scattering at lower temperature (Wang et al., 2018). In addition, 2D Bi$_2$Se$_3$ has demonstrated promising potential in flexible optoelectronic devices because of its inherent atomic structure and excellent flexibility (Liu et al., 2020a, 2020b, 2020c; Peng et al., 2012). As shown in Figure 4G, flexible near-infrared photodetectors based on 2D Bi$_2$Se$_3$ nanosheets using paper as substrate and pencil-drawn graphite as electrodes were fabricated by Qi and co-authors (Liu et al., 2019a, 2019b). The as-fabricated flexible photodetector with various bending curvatures exhibited

excellent stability under 1064 nm laser illumination (Figure 4H). The switching photo-response behavior of the device could be maintained after bending for 1000 cycles (Figure 4I), indicating that the flexible near-infrared photodetectors possessed high durability under bending conditions (Liu et al., 2019a, 2019b). Generally, the high photodetection performance and attractive flexibility pave the way for the application of 2D Bi_2Se_3 in the portable and wearable optoelectronic devices. However, the slow response time at second level is not satisfactory for commercial requirements. It is therefore necessary to carry out more fundamental research to improve the photodetection performance of 2D Bi_2Se_3-based photodetectors.

Except individual Bi_2Se_3, the heterostructures based on 2D Bi_2Se_3 were also demonstrated in the application of photodetection (She et al., 2021; Zhang et al., 2016, 2019, 2020). Zhai et al. reported van der Waals tunneling heterostructure photodetectors composed of 2D Bi_2Se_3 and WSe_2 materials, as shown in Figure 5A (Wang et al., 2020a, 2020b). In this heterostructure, 2D Bi_2Se_3 and WSe_2 formed desirable broken-gap type-III band alignment with high interfacial barriers and efficient charge separation (Figure 5B), which made the 2D Bi_2Se_3/WSe_2 heterostructure exhibit ultralow dark current below picoampere and fast response rate in 4 ms. Moreover, the broken-gap band alignments of the heterostructure enabled photo-generated carriers to transport through overlapped regions by means of direct or Fowler-Nordheim tunneling, forming significant photocurrent. As a result, the 2D Bi_2Se_3/WSe_2 heterostructure presented responsivity of 94.26 A W^{-1} and detectivity of 7.9 × 10^{12} Jones for visible light at 532 nm, and responsivity of 3 A W^{-1} and detectivity of 2.2 × 10^{10} Jones for near-infrared light at 1456 nm (Figure 5C) (Wang et al., 2020a, 2020b). The dark current of the heterostructure was obviously suppressed, but the responsivity still has room for improvement because of the weak optical absorption that originates from its atomically thin nature. In view of this, Zhai and co-authors constructed a hybrid heterostructure by integrating metal-organic frameworks (MOFs) nanoparticles with strong optical absorption on the surface of 2D Bi_2Se_3 flakes (Figure 5D) (Wang et al., 2021a, 2021b, 2021c, 2021d). In this case, the MOF nanoparticles can not only serve as a photosensitive material to absorb incident light, but also act as a photogate layer to regulate the channel conductance of Bi_2Se_3 channel (Figure 5E), thereby enhancing the photoconductivity gain of the device and realizing high-performance photodetection. As displayed in Figure 5F, the resultant photodetector demonstrated outstanding responsivity up to 4725 A W^{-1} with high detectivity of 3.5 × 10^{13} Jones under 1500 nm illumination with power density of 0.012 mW cm^{-2} at V_{ds} = 1 V and V_{gs} = 60 V (Wang et al., 2021a, 2021b, 2021c, 2021d).

Undoubtedly, constructing heterostructures are particularly beneficial for improving the performance and expanding functions of the optoelectronic devices. For instance, 2D rubrene/Bi_2Se_3 organic-inorganic heterostructure (Figure 5G) exhibited a high responsivity of 124 A W^{-1} and a fast response rate of 54 ms with the built-in electric field inhibiting the persistent photoconductivity (PPC) effect of components (Pei et al., 2020). Bi_2Se_3/MoO_3 thin film heterostructure not only possessed high responsivity of 2.61 × 10^3 A W^{-1} with a response speed of up to 63 µs, but also demonstrated brilliant environment stability for up to 100 days without any encapsulation (Figure 5H) (Yang et al., 2020). Besides, the heterogeneous integration of 2D Bi_2Se_3 and graphene achieved mid-infrared photodetection (λ = 3.5 µm) with a high responsivity of 1.97 A W^{-1} at room temperature (Figure 5I) (Kim et al., 2017). These fruitful research progresses and excellent device performance demonstrate the promising potential of 2D Bi_2Se_3 in the application of visible-infrared photodetection.
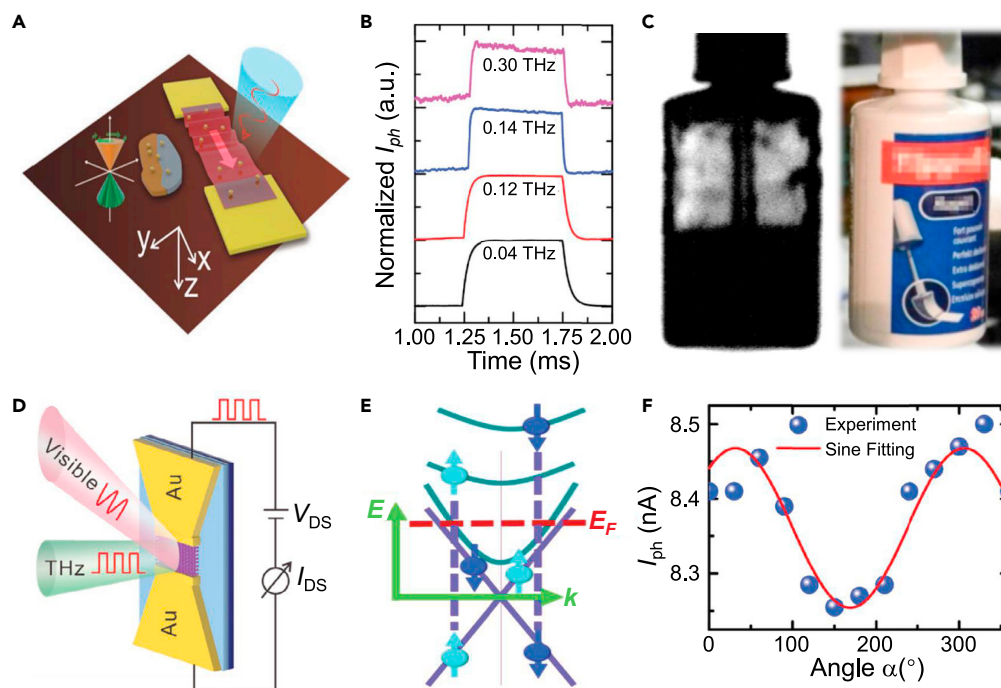
Terahertz detection

Currently, terahertz radiation with frequency range of 0.1–10 THz (corresponding to the wavelength range of 3000-30 µm) is an important topic in promising technological challenges because of its wide applications in communication, noninvasive imaging and other fields related to daily life (Viti et al., 2016). Fabricating high-sensitivity THz detectors is essential for the progressive development of THz technology. In this context, lots of investigations have been conducted to exploit novel materials that could meet the detection requirements (Chen et al., 2016; Yang et al., 2018). Topological insulator Bi_2Se_3 is considered as a promising candidate platform for high-sensitivity THz detection due to the presence of Dirac fermions arising from well-defined topological surface states (Giorgianni et al., 2016; Kamboj et al., 2017; Luo et al., 2019; Zhang et al., 2010). Importantly, the plasmonic excitation of the Dirac fermions lies in the THz range, which makes Bi_2Se_3 exhibit strong THz response (Giorgianni et al., 2016; Kamboj et al., 2017; Luo et al., 2019). As shown in Figure 6A, a demonstration of THz detector based on atomically thin Bi_2Se_3 flake has been fabricated by Cheng and co-authors (Tang et al., 2018). In this device, the incident THz photons were converted into the local surface plasmons at the interface of Bi_2Se_3 and electrodes by the subwavelength metal contacts, thereby driving the Dirac fermions of topological surface states to
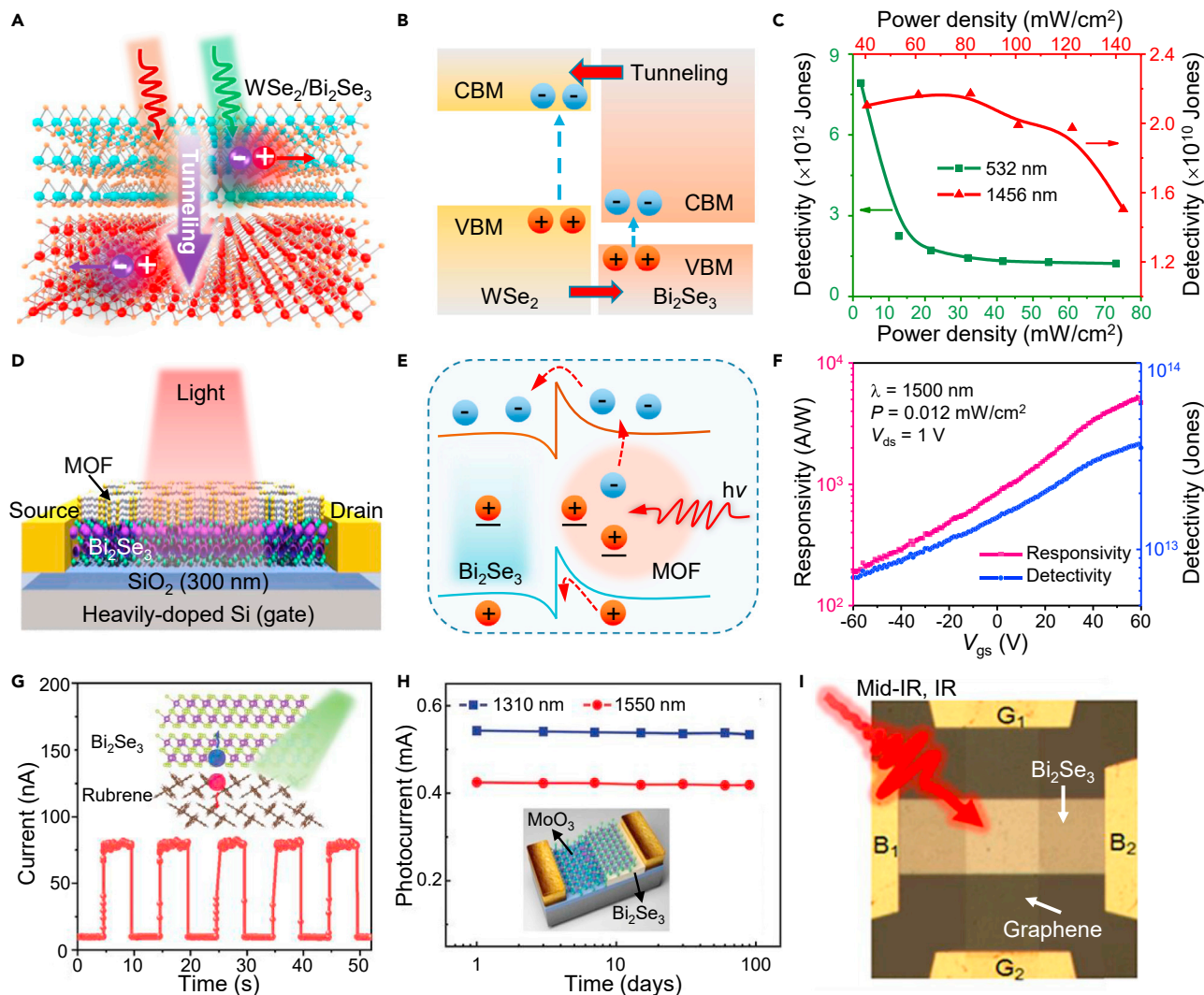
Figure 5. Visible-infrared photodetection of 2D Bi$_2$Se$_3$-based heterostructures

(A) Schematic diagrams of Bi$_2$Se$_3$/WSe$_2$ tunneling heterostructure with electron-hole pair generation and tunneling under illumination.

(B) Energy band diagrams of the Bi$_2$Se$_3$/WSe$_2$ tunneling heterostructure.

(C) Power density-dependent responsivity and detectivity of the heterostructure under 532 nm and 1456 nm illumination. (A–C) Reproduced with permission from (Wang et al., 2020a, 2020b). Copyright 2020 Science China Press and Springer-Verlag GmbH Germany.

(D) Schematic diagram of Bi$_2$Se$_3$/MOF hybrid heterostructure.

(E) Schematic band diagram of the hybrid heterostructure photodetector under illumination.

(F) Gate-dependent responsivity and detectivity of the hybrid heterostructure under 1500 nm illumination. (D–F) Reproduced with permission from (Wang et al., 2021a, 2021b, 2021c, 2021d). Copyright 2021 Science China Press and Springer-Verlag GmbH Germany.

(G) Bi$_2$Se$_3$/Rubrene heterostructure visible photodetector with suppressed photoconductivity effect. Reproduced with permission from (Pei et al., 2020). Copyright 2020 WILEY-VCH Verlag GmbH & Co. KGaA, Weinheim.

(H) Bi$_2$Se$_3$/MoO$_3$ heterostructure infrared photodetector at optical communication waveband, showing long-term environmental stability. Reproduced with permission from. Copyright 2020 WILEY-VCH Verlag GmbH & Co. KGaA, Weinheim.

(I) Bi$_2$Se$_3$/graphene heterostructure mid-infrared photodetector with high sensitivity at room temperature. Reproduced with permission from (Kim et al., 2017). Copyright 2017 American Chemical Society.

move back and forth. The device presented excellent photo-response under irradiation with various frequencies from 0.04 to 0.3 THz (Figure 6B) and demonstrated high sensitivity with a noise-equivalent power of 3.6×10^{-13} W Hz$^{-1/2}$ and a detectivity of 2.17×10^{11} cm W Hz$^{-1/2}$ at room temperature (Tang et al., 2018). In addition, large area THz imaging of a target object (Figure 6C) was achieved by using a Bi$_2$Te$_{2.2}$Se$_{0.8}$-based detector under the impingement of 0.33 THz radiation (Viti et al., 2016).

Figure 6. Terahertz detection based on 2D Bi₂Se₃ flakes
(A) 3D schematics of 2D Bi_2Se_3 terahertz detection principle.
(B) The time-resolved photoresponse of the detector at various frequencies of 0.04 THz to 0.30 THz. (A and B) Reproduced with permission from (Tang et al., 2018). Copyright 2018 WILEY-VCH Verlag GmbH & Co. KGaA, Weinheim.
(C) Terahertz imaging of a glue jar, which was obtained while impinging the 0.33 THz radiation on a $Bi_2Te_{2.2}Se_{0.8}$ detector. Reproduced with permission from (Viti et al., 2016). Copyright 2015 American Chemical Society.
(D) Infrared pumping and probing with THz radiation of the topological surface states in a metal-Bi_2Se_3-metal device.
(E) Physical mechanism of interband transition in topological surface states and bulk states.
(F) Photocurrent of the THz device under various infrared radiation polarization states. (D–F) Reproduced with permission from (Tang et al., 2018). Copyright 2018 WILEY-VCH Verlag GmbH & Co. KGaA, Weinheim.

The topological surface states-related THz response of 2D Bi_2Se_3 flakes was further investigated by visible pumping and probing with THz radiation, as shown in Figure 6D (Tang et al., 2018). The interband transition between topological surface states depended on the excitation with selective rule of spin states because of their locked spin-momentum feature (Figure 6E). Under the excitation of elliptically and circularly polarized pumping light, the Bi_2Se_3-based detector presented well-fitted helicity-dependent THz photo-response (Figure 6F), indicating that the topological surface states dominated the THz response mechanism for topological insulator Bi_2Se_3 (Tang et al., 2018). These results provide valuable references for designing THz detectors by taking advantage of the fascinating physical properties of topological insulators. In follow-up research, the design of THz devices based on 2D Bi_2Se_3 could be incorporated into reconfigurable metasurfaces (metamaterials) to achieve versatile functional devices (Hu et al., 2021).

Opto-spintronic device

Topological surface states of Bi_2Se_3 possess helical Dirac dispersion with spin locked to momentum, which makes it potentially promising for quantum computing spintronics applications (Bhattacharyya et al., 2018a, 2018b; He et al., 2019; Khokhriakov et al., 2020). Numerous studies have demonstrated that topological surface states of topological insulators exhibit novel electronic responses and fascinating optoelectronic effects to polarized light (Besbas et al., 2016; Kastl et al., 2015; Wang et al., 2019a, 2019b, 2019c; Zhuang et al., 2021). Charge carriers with spin-momentum locking on the topological surface states could be selectively excited to photocurrent according to the polarization states of incident light. As shown in Figure 7A, the charge carriers on the topological surface states formed pure spin currents without a net flow of charge in equilibrium (McIver et al., 2011). Under excitation with circularly polarized light, these pure spin currents were transformed into spin-polarized electrical
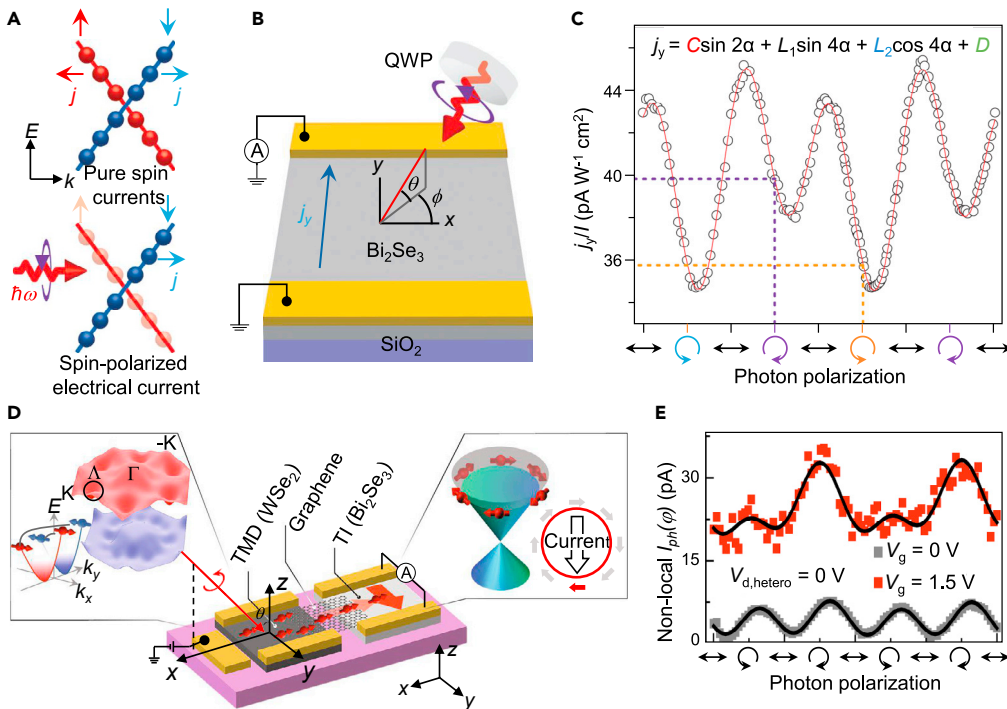
Figure 7. Spin-optoelectronic devices based on 2D Bi$_2$Se$_3$ flakes

(A) Pure spin currents from the topological surface states of Bi$_2$Se$_3$ in equilibrium and spin-polarized electrical current induced by driving the topological surface states with circularly polarized light.

(B) Schematic diagram of spin-polarized electrical current measurement.

(C) Photon polarization-dependent spin-polarized electrical current originating from the helical Dirac fermions of Bi$_2$Se$_3$.

(A–C) Reproduced with permission from (McIver et al., 2011). Copyright 2012 Macmillan Publishers Limited.

(D) 3D device scheme of the valley-locked spin photocurrent measurement in a Bi$_2$Se$_3$-graphen-WSe$_2$ heterostructure.

(E) Helicity-dependent photocurrent of the heterostructure. (D and E) Reproduced with permission from (Cha et al., 2018). Copyright 2018 Springer Nature.

current because of the out of equilibrium topological surface states. The microscopic origin of this phenomenon is related to the interband transitions between topological surface states, which are dependent on the surface state spin orientation. Because the the bulk states of Bi$_2$Se$_3$ were spin-degenerate, the photo helicity-dependent photocurrents can only be contributed by the surface states (Figure 7B). By rotating the quarter-wave plate to change the photon polarization between left-circular and right-circular, the polarization-dependent photocurrents were measured in the opto-spintronic device (Figure 7C) (McIver et al., 2011). The helicity-dependent photocurrents in Bi$_2$Se$_3$ could be modulated by the application of ionic liquid gate (Duan et al., 2014), suggesting that there are many possibilities for the regulation of spin-polarized photocurrents.

Recently, Choi et al. reported a lateral heterostructure opto-spintronic device composed of Bi$_2$Se$_3$, graphene and WSe$_2$ for the demonstration of generation, transport and detection of valley-locked spin photocurrent (Cha et al., 2018). In this configuration (Figure 7D), the WSe$_2$ flake was used for the optical generation and electrical regulation of valley-locked spin-polarized carriers, graphene served as the carrier transport channel and Bi$_2$Se$_3$ played the role in detecting spin-polarized carriers. Under the excitation of circularly polarized light, valley-locked spin-polarized carriers generated in inversion-symmetry-broken WSe$_2$ induced by electrostatic gating. The as-generated carriers were transferred into Bi$_2$Se$_3$ through the submicrometre-long graphene channel. Benefiting from the unique spin-momentum locking property of Bi$_2$Se$_3$, the polarity of current detected in Bi$_2$Se$_3$ was able to reflect the characteristics of valley-locked spin carriers. Analogously, helicity-resolved photocurrents shown in Figure 7E were measured by changing the polarization of incident photons (Cha et al., 2018). From these advances, it can be seen that combining the topological surface states of topological insulators and the valleytronics of transition metal chalcogenides provides a suitable platform for manipulating the degrees of freedom of carriers.
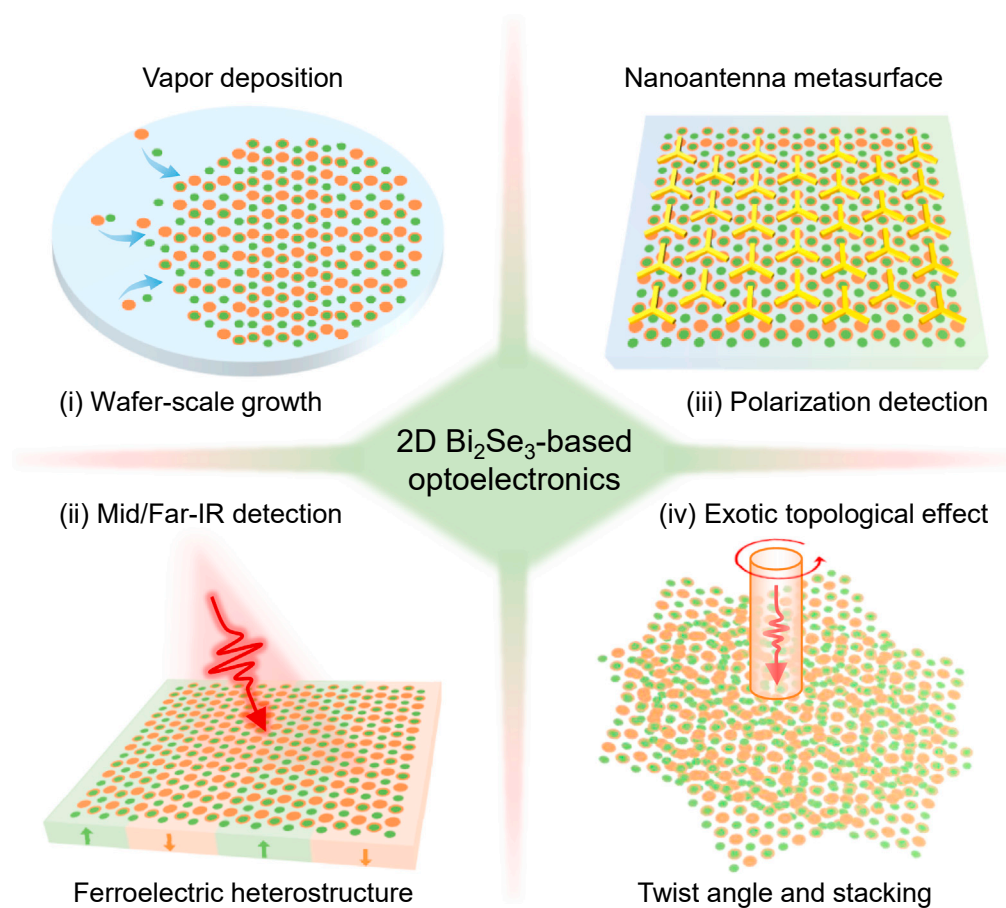
Figure 8. Prospects for 2D Bi$_2$Se$_3$-based optoelectronics, covering wafer-scale growth, mid/far-infrared detection, polarization detection and exotic topological effects

CHALLENGES AND PROSPECTS

Extensive scientific explorations have been carried out on 2D Bi$_2$Se$_3$ materials, including physical property disclosure, material preparation, and device application. This review presents an overview of the structure and properties, preparation approaches (solution synthesis and van der Waals epitaxy growth), and device applications (visible-infrared photodetection, terahertz detection and opto-spintronic device) of 2D Bi$_2$Se$_3$ materials. These findings indicate that 2D Bi$_2$Se$_3$ is a promising candidate for optoelectronic applications. Despite rapid progress have been made so far, there are still several technical challenges that need to be addressed.

The potential solutions for the development of 2D Bi$_2$Se$_3$ materials are summarized in Figure 8. From the perspective of material level, wafer-scale preparation of 2D Bi$_2$Se$_3$ materials with high crystallinity, controllable thickness, and uniform orientation is a prerequisite for optoelectronic devices in the real-world applications. It is therefore of significant importance to develop new routes to grow wafer-scale 2D Bi$_2$Se$_3$ materials. Judging from the current research progress, the vapor deposition method is a very promising way to produce large-area high-quality 2D materials (Liu and Zhai, 2020; Sun et al., 2021; Tong et al., 2019). Selenization of pre-deposited Bi thin film with subsequent heat treatment may be an effective route to fabricate wafer-scale 2D Bi$_2$Se$_3$ materials (Liu et al., 2020a, 2020b, 2020c; Yu et al., 2018). This requires theoretical calculations to deeply understand the thermodynamics and kinetics of crystal nucleation and growth.

In the aspect of device fabrication, high-performance multifunctional devices are always pursued in the field of optoelectronics. There is still huge room for improvement in the device performance and function demonstration of existing 2D Bi$_2$Se$_3$-based optoelectronic devices. It is urgent to focus on device performance improvement and innovative device concepts. Constructing ferroelectric heterostructure by combining 2D Bi$_2$Se$_3$ with ferroelectric material is expected to manipulate the carrier concentration and

suppress the dark current of optoelectronic device for the purpose of achieving high sensitivity (Luo et al., 2021a, 2021b; Lv et al., 2019; Wu et al., 2020). In the meanwhile, an extended feature of mid/far-infrared detection in this heterostructure may be obtained by exploiting the inherent thermoelectric property of Bi_2Se_3 and pyroelectric character of ferroelectric material (Gopalan et al., 2017; Shimatani et al., 2019; Wang et al., 2019a, 2019b, 2019c). In addition, the integration of metamaterials with different configurations on the surface of 2D Bi_2Se_3 may also bring some exciting results. In this case, local plasmon resonance could be generated in the nanoantenna metasurface under light illumination, which would enhance the light-matter interaction and improve the responsivity of device (Fang et al., 2012; Li et al., 2020a, 2020b; Wei et al., 2020). Moreover, the metasurface-mediated optoelectronic devices possess potential applications in calibration-free polarization detection and filterless full-Stokes detection, because the exotic properties of metamaterials imbue them with unique functions such as the dependence on wavelength, chirality, polarization and angle of incidence (Fan et al., 2021; Wei et al., 2020, 2021).

Apart from working on the material preparation and device fabrication, exploring fundamental physics of 2D Bi_2Se_3 is required to disclose unpredictable exotic topological effects. The presence of topological surface states in Bi_2Se_3 predestines it for the fundamental study of condensed matter physics. For example, introducing magnetic order in Bi_2Se_3 by doping with magnetic substances could open the topological surface states, leading to various interesting physical phenomena such as quantum anomalous Hall effect and topological magnetoelectric effect (Chen et al., 2019; Fan et al., 2016; Jiang et al., 2020; Tokura et al., 2019; Wang et al., 2021a, 2021b, 2021c, 2021d). Fabricating van der Waals heterostructures by stacking topological insulator Bi_2Se_3 with (anti)ferromagnetic semiconductors may be a feasible route to study magnetic proximity effect and topological Hall effect due to the existence of magnetic proximity effect in such configurations (He et al., 2017; Hou et al., 2019; Katmis et al., 2016; Li et al., 2021a, 2021b; Luo and Qi, 2013; Zhuang et al., 2021). In addition, it should be possible to create a moiré superlattice by twisting Bi_2Se_3. Similar to magic-angle graphene, the induced moiré superlattice may lead to surprising physical effects, such as the coveted superconductivity, Skyrmions and more (Cao et al., 2018a; 2018b; Li et al., 2021a, 2021b; Stepanov et al., 2020; Uri et al., 2020; Zhang and Liu, 2021). The combination of these novel properties and fantastic photonics will lead to more unpredictable topological effects.

In conclusion, the journey of exploring 2D Bi_2Se_3-based optoelectronics is still in its infancy. The future technological advancement of 2D Bi_2Se_3-based optoelectronics requires a holistic collaborative approach across different disciplines including materials science, physics, photonics, electronics and spintronics.

AUTHOR CONTRIBUTIONS

T. Y. Z conceived the idea, F. K. W prepared the figures and wrote the manuscript. S. J. Y revised the manuscript. All authors participated in the discussion and revised the manuscript.

DECLARATION OF INTERESTS

The authors declare no competing interests.

REFERENCES

Akinwande, D., Huyghebaert, C., Wang, C.H., Serna, M.I., Goossens, S., Li, L.J., Wong, H.P., and Koppens, F.H.L. (2019). Graphene and two-dimensional materials for silicon technology. Nature 573, 507.

Akinwande, D., Petrone, N., and Hone, J. (2014). Two-dimensional flexible nanoelectronics. Nat. Commun. 5, 5678.

Bansal, N., Kim, Y.S., Brahlek, M., Edrey, E., and Oh, S. (2012). Thickness-independent transport channels in topological insulator Bi_2Se_3 thin films. Phys. Rev. Lett. 109, 116804.

Besbas, J., Banerjee, K., Son, J., Wang, Y., Wu, Y., Brahlek, M., Koirala, N., Moon, J., Seongshik, O., and Yang, H. (2016). Helicity-dependent photovoltaic effect in Bi_2Se_3 under normal incident light. Adv. Opt. Mater. 4, 1642.

Bhattacharyya, B., Awana, V.P.S., Senguttuvan, T.D., Ojha, V.N., and Husale, S. (2018a). Proximity-induced supercurrent through topological insulator based nanowires for quantum computation studies. Sci. Rep. 8, 17237.

Bhattacharyya, B., Gupta, A., Senguttuvan, T.D., Ojha, V.N., and Husale, S. (2018b). Topological insulator based dual state photo-switch originating through bulk and surface conduction channels. Phys. Status Solidi B 255, 800340.

Bhattacharyya, B., Sharma, A., Awana, V.P., Srivastava, A.K., Senguttuvan, T.D., and Husale, S. (2017a). Observation of quantum oscillations in

FIB fabricated nanowires of topological insulator (Bi_2Se_3). J. Phys. Condens. Matter. *29*, 115602.

Bhattacharyya, B., Sharma, A., Sinha, B., Shah, K., Jejurikar, S., Senguttuvan, T.D., and Husale, S. (2017b). Evidence of robust 2D transport and Efros-Shklovskii variable range hopping in disordered topological insulator (Bi_2Se_3) nanowires. Sci. Rep. *7*, 7825.

Bianchi, M., Guan, D., Bao, S., Mi, J., Iversen, B.B., King, P.D., and Hofmann, P. (2010). Coexistence of the topological state and a two-dimensional electron gas on the surface of Bi_2Se_3. Nat. Commun. *1*, 128.

Cai, Z., Liu, B., Zou, X., and Cheng, H.M. (2018). Chemical vapor deposition growth and applications of two-dimensional materials and their heterostructures. Chem. Rev. *118*, 6091.

Cao, Y., Fatemi, V., Demir, A., Fang, S., Tomarken, S.L., Luo, J.Y., Sanchez-Yamagishi, J.D., Watanabe, K., Taniguchi, T., Kaxiras, E., et al. (2018a). Correlated insulator behaviour at half-filling in magic-angle graphene superlattices. Nature *556*, 80.

Cao, Y., Fatemi, V., Fang, S., Watanabe, K., Taniguchi, T., Kaxiras, E., and Jarillo-Herrero, P. (2018b). Unconventional superconductivity in magic-angle graphene superlattices. Nature *556*, 43.

Cha, S., Noh, M., Kim, J., Son, J., Bae, H., Lee, D., Kim, H., Lee, J., Shin, H.S., Sim, S., et al. (2018). Generation, transport and detection of valley-locked spin photocurrent in WSe_2-graphene-Bi_2Se_3 heterostructures. Nat. Nanotechnol. *13*, 910.

Chen, B., Fei, F., Zhang, D., Zhang, B., Liu, W., Zhang, S., Wang, P., Wei, B., Zhang, Y., Zuo, Z., et al. (2019). Intrinsic magnetic topological insulator phases in the Sb doped $MnBi_2Te_4$ bulks and thin flakes. Nat. Commun. *10*, 4469.

Chen, H., Liu, H., Zhang, Z., Hu, K., and Fang, X. (2016). Nanostructured photodetectors: from ultraviolet to terahertz. Adv. Mater. *28*, 403.

Chen, X., Ma, X.C., He, K., Jia, J.F., and Xue, Q.K. (2011). Molecular beam epitaxial growth of topological insulators. Adv. Mater. *23*, 1162.

Cho, S., Butch, N.P., Paglione, J., and Fuhrer, M.S. (2011). Insulating behavior in ultrathin bismuth selenide field effect transistors. Nano Lett. *11*, 1925.

Dang, W., Peng, H., Li, H., Wang, P., and Liu, Z. (2010). Epitaxial heterostructures of ultrathin topological insulator nanoplate and graphene. Nano Lett. *10*, 2870.

Dankert, A., Geurs, J., Kamalakar, M.V., Charpentier, S., and Dash, S.P. (2015). Room temperature electrical detection of spin polarized currents in topological insulators. Nano Lett. *15*, 7976.

Duan, J., Tang, N., He, X., Yan, Y., Zhang, S., Qin, X., Wang, X., Yang, X., Xu, F., Chen, Y., et al. (2014). Identification of helicity-dependent photocurrents from topological surface states in Bi_2Se_3 gated by ionic liquid. Sci. Rep. *4*, 4889.

Fan, J., Zhang, L., Wei, S., Zhang, Z., Choi, S.-K., Song, B., and Shi, Y. (2021). A review of additive manufacturing of metamaterials and developing trends. Mater. Today. https://doi.org/10.1016/j.mattod.2021.04.019.

Fan, Y., Kou, X., Upadhyaya, P., Shao, Q., Pan, L., Lang, M., Che, X., Tang, J., Montazeri, M., Murata, K., et al. (2016). Electric-field control of spin-orbit torque in a magnetically doped topological insulator. Nat. Nanotechnol. *11*, 352.

Fang, Y., Wang, F., Wang, R., Zhai, T., and Huang, F. (2021). 2D $NbOI_2$: a chiral semiconductor with highly in-plane anisotropic electrical and optical properties. Adv. Mater. *33*, 2101505.

Fang, Z., Liu, Z., Wang, Y., Ajayan, P.M., Nordlander, P., and Halas, N.J. (2012). Graphene-antenna sandwich photodetector. Nano Lett. *12*, 3808.

Giorgianni, F., Chiadroni, E., Rovere, A., Cestelli-Guidi, M., Perucchi, A., Bellaveglia, M., Castellano, M., Di Giovenale, D., Di Pirro, G., Ferrario, M., et al. (2016). Strong nonlinear terahertz response induced by Dirac surface states in Bi_2Se_3 topological insulator. Nat. Commun. *7*, 11421.

Gopalan, K.K., Janner, D., Nanot, S., Parret, R., Lundeberg, M.B., Koppens, F.H.L., and Pruneri, V. (2017). Mid-infrared pyroresistive graphene detector on $LiNbO_3$. Adv. Opt. Mater. *5*, 1600723.

Guo, Y., Aisijiang, M., Zhang, K., Jiang, W., Chen, Y., Zheng, W., Song, Z., Cao, J., Liu, Z., and Peng, H. (2013). Selective-area van der Waals epitaxy of topological insulator grid nanostructures for broadband transparent flexible electrodes. Adv. Mater. *25*, 5959.

Guo, Y., Liu, Z., and Peng, H. (2015). A roadmap for controlled production of topological insulator nanostructures and thin films. Small *11*, 3290.

Han, W., Huang, P., Li, L., Wang, F., Luo, P., Liu, K., Zhou, X., Li, H., Zhang, X., Cui, Y., and Zhai, T. (2019a). Two-dimensional inorganic molecular crystals. Nat. Commun. *10*, 4728.

Han, W., Liu, K., Yang, S., Wang, F., Su, J., Jin, B., Li, H., and Zhai, T. (2019b). Salt-assisted chemical vapor deposition of two-dimensional materials. Sci. China Chem. *62*, 1300.

He, K., Zhang, Y., He, K., Chang, C.-Z., Song, C.-L., Wang, L.-L., Chen, X., Jia, J.-F., Fang, Z., Dai, X., et al. (2010). Crossover of the three-dimensional topological insulator Bi_2Se_3 to the two-dimensional limit. Nat. Phys. *6*, 584.

He, L., Xiu, F., Yu, X., Teague, M., Jiang, W., Fan, Y., Kou, X., Lang, M., Wang, Y., Huang, G., et al. (2012). Surface-dominated conduction in a 6 nm thick Bi_2Se_3 thin film. Nano Lett. *12*, 1486.

He, M., Sun, H., and He, Q.L. (2019). Topological insulator: spintronics and quantum computations. Front. Phys. *14*, 43401.

He, Q.L., Kou, X., Grutter, A.J., Yin, G., Pan, L., Che, X., Liu, Y., Nie, T., Zhang, B., Disseler, S.M., et al. (2017). Tailoring exchange couplings in magnetic topological-insulator/antiferromagnet heterostructures. Nat. Mater. *16*, 94.

Hong, S.B., Kim, D.K., Chae, J., Kim, K., Jeong, K., Kim, J., Park, H., Yi, Y., and Cho, M.H. (2020). Enhanced photoinduced carrier generation efficiency through surface band bending in topological insulator Bi_2Se_3 thin films by the oxidized layer. ACS Appl. Mater. Interfaces *12*, 26649.

Hong, S.S., Kundhikanjana, W., Cha, J.J., Lai, K., Kong, D., Meister, S., Kelly, M.A., Shen, Z.X., and Cui, Y. (2010). Ultrathin topological insulator Bi_2Se_3 nanoribbons exfoliated by atomic force microscopy. Nano Lett. *10*, 3118.

Hou, Y., Kim, J., and Wu, R. (2019). Magnetizing topological surface states of Bi_2Se_3 with a CrI_3 monolayer. Sci. Adv. *5*, eaaw1874.

Hsieh, D., Xia, Y., Qian, D., Wray, L., Dil, J.H., Meier, F., Osterwalder, J., Patthey, L., Checkelsky, J.G., Ong, N.P., et al. (2009). A tunable topological insulator in the spin helical Dirac transport regime. Nature *460*, 1101.

Hu, Y., Tong, M., Cheng, X., Zhang, J., Hao, H., You, J., Zheng, X., and Jiang, T. (2021). Bi_2Se_3-functionalized metasurfaces for ultrafast all-optical switching and efficient modulation of terahertz waves. ACS Photon. *8*, 771.

Iannaccone, G., Bonaccorso, F., Colombo, L., and Fiori, G. (2018). Quantum engineering of transistors based on 2D materials heterostructures. Nat. Nanotechnol. *13*, 183.

Jiang, J., Xiao, D., Wang, F., Shin, J.H., Andreoli, D., Zhang, J., Xiao, R., Zhao, Y.F., Kayyalha, M., Zhang, L., et al. (2020). Concurrence of quantum anomalous Hall and topological Hall effects in magnetic topological insulator sandwich heterostructures. Nat. Mater. *19*, 732.

Kamboj, V.S., Singh, A., Ferrus, T., Beere, H.E., Duffy, L.B., Hesjedal, T., Barnes, C.H.W., and Ritchie, D.A. (2017). Probing the topological surface state in Bi_2Se_3 thin films using temperature-dependent terahertz spectroscopy. ACS Photon. *4*, 2711.

Kastl, C., Karnetzky, C., Karl, H., and Holleitner, A.W. (2015). Ultrafast helicity control of surface currents in topological insulators with near-unity fidelity. Nat. Commun. *6*, 6617.

Katmis, F., Lauter, V., Nogueira, F.S., Assaf, B.A., Jamer, M.E., Wei, P., Satpati, B., Freeland, J.W., Eremin, I., Heiman, D., et al. (2016). A high-temperature ferromagnetic topological insulating phase by proximity coupling. Nature *533*, 513.

Khokhriakov, D., Hoque, A.M., Karpiak, B., and Dash, S.P. (2020). Gate-tunable spin-galvanic effect in graphene-topological insulator van der Waals heterostructures at room temperature. Nat. Commun. *11*, 3657.

Kim, D., Cho, S., Butch, N.P., Syers, P., Kirshenbaum, K., Adam, S., Paglione, J., and Fuhrer, M.S. (2012). Surface conduction of topological Dirac electrons in bulk insulating Bi_2Se_3. Nat. Phys. *8*, 460.

Kim, D., Syers, P., Butch, N.P., Paglione, J., and Fuhrer, M.S. (2014). Ambipolar surface state thermoelectric power of topological insulator Bi_2Se_3. Nano Lett. *14*, 1701.

Kim, J., Park, S., Jang, H., Koirala, N., Lee, J.-B., Kim, U.J., Lee, H.-S., Roh, Y.-G., Lee, H., Sim, S., et al. (2017). Highly sensitive, gate-tunable, room-temperature mid-infrared photodetection based on graphene-Bi_2Se_3 heterostructure. ACS Photon. *4*, 482.

Kong, D., and Cui, Y. (2011). Opportunities in chemistry and materials science for topological insulators and their nanostructures. Nat. Chem. *3*, 845.

Kong, D., Dang, W., Cha, J.J., Li, H., Meister, S., Peng, H., Liu, Z., and Cui, Y. (2010). Few-layer nanoplates of Bi_2Se_3 and Bi_2Te_3 with highly tunable chemical potential. Nano Lett. *10*, 2245.

Koppens, F.H., Mueller, T., Avouris, P., Ferrari, A.C., Vitiello, M.S., and Polini, M. (2014). Photodetectors based on graphene, other two-dimensional materials and hybrid systems. Nat. Nanotechnol. *9*, 780.

Li, H., Cao, J., Zheng, W., Chen, Y., Wu, D., Dang, W., Wang, K., Peng, H., and Liu, Z. (2012). Controlled synthesis of topological insulator nanoplate arrays on mica. J. Am. Chem. Soc. *134*, 6132.

Li, H., Li, Y., Aljarb, A., Shi, Y., and Li, L.J. (2017). Epitaxial growth of two-dimensional layered transition-metal dichalcogenides: growth mechanism, controllability, and scalability. Chem. Rev. *118*, 6134.

Li, J., Yang, X., Liu, Y., Huang, B., Wu, R., Zhang, Z., Zhao, B., Ma, H., Dang, W., Wei, Z., et al. (2020a). General synthesis of two-dimensional van der Waals heterostructure arrays. Nature *579*, 368.

Li, L., Wang, J., Kang, L., Liu, W., Yu, L., Zheng, B., Brongersma, M.L., Werner, D.H., Lan, S., Shi, Y., et al. (2020b). Monolithic full-Stokes near-infrared polarimetry with chiral plasmonic metasurface integrated graphene-silicon photodetector. ACS Nano *14*, 16634.

Li, C.-K., Yao, X.-P., and Chen, G. (2021a). Twisted magnetic topological insulators. Phys. Rev. Res. *3*, 033156.

Li, P., You, Y.W., Huang, K., and Luo, W. (2021b). Quantum anomalous Hall effect in $Cr_2Ge_2Te_6$/Bi_2Se_3/$Cr_2Ge_2Te_6$ heterostructures. J. Phys. Condens. Matter. https://doi.org/10.1088/1361-648X/ac2117.

Liang, S.J., Cheng, B., Cui, X., and Miao, F. (2019). Van der Waals heterostructures for high-performance device applications: challenges and opportunities. Adv. Mater. *31*, 1903800.

Liu, C., Chen, H., Wang, S., Liu, Q., Jiang, Y.G., Zhang, D.W., Liu, M., and Zhou, P. (2020a). Two-dimensional materials for next-generation computing technologies. Nat. Nanotechnol. *15*, 545.

Liu, J.L., Chen, H., Li, X., Wang, H., Zhang, Z.K., Pan, W.W., Yuan, G., Ren, Y.L., and Lei, W. (2020b). Ultra-fast and high flexibility near-infrared photodetectors based on Bi_2Se_3 nanobelts grown via catalyst-free van der Waals epitaxy. J. Alloy. Compd. *818*, 152819.

Liu, S., Huang, Z., Qiao, H., Hu, R., Ma, Q., Huang, K., Li, H., and Qi, X. (2020c). Two-dimensional Bi_2Se_3 nanosheet based flexible infrared photodetector with pencil-drawn graphite electrodes on paper. Nanoscale Adv. *2*, 906.

Liu, L., and Zhai, T. (2020). Wafer-scale vertical van der Waals heterostructures. InfoMat *3*, 3.

Liu, Y., Cao, L., Zhong, J., Yu, J., He, J., and Liu, Z. (2019a). Synthesis of bismuth selenide nanoplates by solvothermal methods and its stacking optical properties. J. Appl. Phys. *125*, 035302.

Liu, Y., Huang, Y., and Duan, X. (2019b). Van der Waals integration before and beyond two-dimensional materials. Nature *567*, 323.

Liu, R., Wang, F., Liu, L., He, X., Chen, J., Li, Y., and Zhai, T. (2021a). Band alignment engineering in two-dimensional transition metal dichalcogenide-based heterostructures for photodetectors. Small Struct. *2*, 2000136.

Liu, Y., Duan, X., Shin, H.J., Park, S., Huang, Y., and Duan, X. (2021b). Promises and prospects of two-dimensional transistors. Nature *591*, 43.

Liu, Y., Li, Y.Y., Rajput, S., Gilks, D., Lari, L., Galindo, P.L., Weinert, M., Lazarov, V.K., and Li, L. (2014). Tuning Dirac states by strain in the topological insulator Bi_2Se_3. Nat. Phys. *10*, 294.

Luo, L., Yang, X., Liu, X., Liu, Z., Vaswani, C., Cheng, D., Mootz, M., Zhao, X., Yao, Y., Wang, C.Z., et al. (2019). Ultrafast manipulation of topologically enhanced surface transport driven by mid-infrared and terahertz pulses in Bi_2Se_3. Nat. Commun. *10*, 607.

Luo, S., Li, J., Sun, T., Liu, X., Wei, D., Zhou, D., Shen, J., and Wei, D. (2021a). High-performance mid-infrared photodetection based on Bi_2Se_3 maze and free-standing nanoplates. Nanotechnology *32*, 105705.

Luo, Z.D., Yang, M.M., Liu, Y., and Alexe, M. (2021b). Emerging opportunities for 2D semiconductor/ferroelectric transistor-structure devices. Adv. Mater. *33*, 2005620.

Luo, W., and Qi, X.-L. (2013). Massive Dirac surface states in topological insulator/magnetic insulator heterostructures. Phys. Rev. B *87*, 085431.

Lv, L., Zhuge, F., Xie, F., Xiong, X., Zhang, Q., Zhang, N., Huang, Y., and Zhai, T. (2019). Reconfigurable two-dimensional optoelectronic devices enabled by local ferroelectric polarization. Nat. Commun. *10*, 3331.

Maiti, P.S., Ghosh, S., Leitus, G., Houben, L., and Bar Sadan, M. (2021). Oriented attachment of 2D nanosheets: the case of few-layer Bi_2Se_3. Chem. Mater. *33*, 7558.

McIver, J.W., Hsieh, D., Steinberg, H., Jarillo-Herrero, P., and Gedik, N. (2011). Control over topological insulator photocurrents with light polarization. Nat. Nanotechnol. *7*, 96.

Min, Y., Moon, G.D., Kim, B.S., Lim, B., Kim, J.S., Kang, C.Y., and Jeong, U. (2012). Quick, controlled synthesis of ultrathin Bi_2Se_3 nanodiscs and nanosheets. J. Am. Chem. Soc. *134*, 2872.

Pei, K., Wang, F., Han, W., Yang, S., Liu, K., Liu, K., Li, H., and Zhai, T. (2020). Suppression of persistent photoconductivity of rubrene crystals using gate-tunable rubrene/Bi_2Se_3 diodes with photoinduced negative differential resistance. Small *16*, 2002312.

Peng, H., Dang, W., Cao, J., Chen, Y., Wu, D., Zheng, W., Li, H., Shen, Z.X., and Liu, Z. (2012). Topological insulator nanostructures for near-infrared transparent flexible electrodes. Nat. Chem. *4*, 281.

Peng, H., Lai, K., Kong, D., Meister, S., Chen, Y., Qi, X.L., Zhang, S.C., Shen, Z.X., and Cui, Y. (2010). Aharonov-Bohm interference in topological insulator nanoribbons. Nat. Mater. *9*, 225.

Post, K.W., Chapler, B.C., He, L., Kou, X., Wang, K.L., and Basov, D.N. (2013). Thickness-dependent bulk electronic properties in Bi_2Se_3 thin films revealed by infrared spectroscopy. Phys. Rev. B *88*, 075121.

Pradhan, B., Dalui, A., Paul, S., Roy, D., and Acharya, S. (2020). Solution phase synthesis of large-area ultra-thin two dimensional layered Bi_2Se_3: role of Cu-intercalation and substitution. Mater. Res. Express *6*, 124005.

Ricciardulli, A.G., Yang, S., Smet, J.H., and Saliba, M. (2021). Emerging perovskite monolayers. Nat. Mater. https://doi.org/10.1038/s41563-021-01029-9.

Sacepe, B., Oostinga, J.B., Li, J., Ubaldini, A., Couto, N.J., Giannini, E., and Morpurgo, A.F. (2011). Gate-tuned normal and superconducting transport at the surface of a topological insulator. Nat. Commun. *2*, 575.

Sharma, A., Bhattacharyya, B., Srivastava, A.K., Senguttuvan, T.D., and Husale, S. (2016). High performance broadband photodetector using fabricated nanowires of bismuth selenide. Sci. Rep. *6*, 19138.

Sharma, A., Senguttuvan, T.D., Ojha, V.N., and Husale, S. (2019). Novel synthesis of topological insulator based nanostructures (Bi_2Te_3) demonstrating high performance photodetection. Sci. Rep. *9*, 3804.

She, Y., Wu, Z., You, S., Du, Q., Chu, X., Niu, L., Ding, C., Zhang, K., Zhang, L., and Huang, S. (2021). Multiple-dimensionally controllable nucleation sites of two-dimensional WS_2/Bi_2Se_3 heterojunctions based on vapor growth. ACS Appl. Mater. Interfaces *13*, 15518.

Shimatani, M., Ogawa, S., Fukushima, S., Okuda, S., Kanai, Y., Ono, T., and Matsumoto, K. (2019). Enhanced photogating via pyroelectric effect induced by insulator layer for high-responsivity long-wavelength infrared graphene-based photodetectors operating at room temperature. Appl. Phys. Express *12*, 025001.

Sierra, J.F., Fabian, J., Kawakami, R.K., Roche, S., and Valenzuela, S.O. (2021). Van der Waals heterostructures for spintronics and opto-spintronics. Nat. Nanotechnol. *16*, 856.

Steinberg, H., Gardner, D.R., Lee, Y.S., and Jarillo-Herrero, P. (2010). Surface state transport and ambipolar electric field effect in Bi_2Se_3 nanodevices. Nano Lett. *10*, 5032.

Stepanov, P., Das, I., Lu, X., Fahimniya, A., Watanabe, K., Taniguchi, T., Koppens, F.H.L., Lischner, J., Levitov, L., and Efetov, D.K. (2020). Untying the insulating and superconducting orders in magic-angle graphene. Nature *583*, 375.

Sun, L., Yuan, G., Gao, L., Yang, J., Chhowalla, M., Gharahcheshmeh, M.H., Gleason, K.K., Choi, Y.S., Hong, B.H., and Liu, Z. (2021). Chemical vapour deposition. Nat. Rev. Methods Primers *1*, 5.

Tang, W., Politano, A., Guo, C., Guo, W., Liu, C., Wang, L., Chen, X., and Lu, W. (2018). Ultrasensitive room-temperature terahertz direct

detection based on a bismuth selenide topological insulator. Adv. Funct. Mater. 28, 1801786.

Tokura, Y., Yasuda, K., and Tsukazaki, A. (2019). Magnetic topological insulators. Nat. Rev. Phys. 1, 126.

Tong, X., Liu, K., Zeng, M., and Fu, L. (2019). Vapor-phase growth of high-quality wafer-scale two-dimensional materials. InfoMat 1, 460.

Uri, A., Grover, S., Cao, Y., Crosse, J.A., Bagani, K., Rodan-Legrain, D., Myasoedov, Y., Watanabe, K., Taniguchi, T., Moon, P., et al. (2020). Mapping the twist-angle disorder and Landau levels in magic-angle graphene. Nature 581, 47.

Varoon, K., Zhang, X., Elyassi, B., Brewer, D.D., Gettel, M., Kumar, S., Lee, J.A., Maheshwari, S., Mittal, A., Sung, C.Y., et al. (2011). Dispersible exfoliated zeolite nanosheets and their application as a selective membrane. Science 334, 72.

Viti, L., Coquillat, D., Politano, A., Kokh, K.A., Aliev, Z.S., Babanly, M.B., Tereshchenko, O.E., Knap, W., Chulkov, E.V., and Vitiello, M.S. (2016). Plasma-wave terahertz detection mediated by topological insulators surface states. Nano Lett. 16, 80.

Wang, F., Li, L., Huang, W., Li, L., Jin, B., Li, H., and Zhai, T. (2018). Submillimeter 2D Bi$_2$Se$_3$ flakes toward high-performance infrared photodetection at optical communication wavelength. Adv. Funct. Mater. 28, 1802707.

Wang, F., Luo, P., Zhang, Y., Huang, Y., Zhang, Q., Li, Y., and Zhai, T. (2020a). Band structure engineered tunneling heterostructures for high-performance visible and near-infrared photodetection. Sci. China Mater. 63, 1537.

Wang, F., Zhang, Z., Zhang, Y., Nie, A., Zhao, W., Wang, D., Huang, F., and Zhai, T. (2020b). Honeycomb RhI$_3$ flakes with high environmental stability for optoelectronics. Adv. Mater. 32, 2001979.

Wang, F., Pei, K., Li, Y., Li, H., and Zhai, T. (2021a). 2D homojunctions for electronics and optoelectronics. Adv. Mater. 33, 2005303.

Wang, F., Wang, X., Zhao, Y.F., Xiao, D., Zhou, L.J., Liu, W., Zhang, Z., Zhao, W., Chan, M.H.W., Samarth, N., et al. (2021b). Interface-induced sign reversal of the anomalous Hall effect in magnetic topological insulator heterostructures. Nat. Commun. 12, 79.

Wang, F., Wu, J., Zhang, Y., Yang, S., Zhang, N., Li, H., and Zhai, T. (2021c). High-sensitivity shortwave infrared photodetectors of metal-organic frameworks integrated on 2D layered materials. Sci. China Mater. https://doi.org/10.1007/s40843-021-1781-y.

Wang, F., Yang, S., Wu, J., Hu, X., Li, Y., Li, H., Liu, X., Luo, J., and Zhai, T. (2021d). Emerging two-dimensional bismuth oxychalcogenides for electronics and optoelectronics. InfoMat. https://doi.org/10.1002/inf2.12215.

Wang, M., Wu, J., Lin, L., Liu, Y., Deng, B., Guo, Y., Lin, Y., Xie, T., Dang, W., Zhou, Y., and Peng, H. (2016). Chemically engineered substrates for patternable growth of two-dimensional chalcogenide crystals. ACS Nano 10, 10317.

Wang, F., Zhang, Y., Gao, Y., Luo, P., Su, J., Han, W., Liu, K., Li, H., and Zhai, T. (2019a). 2D metal chalcogenides for IR photodetection. Small 15, 1901347.

Wang, X., Shen, H., Chen, Y., Wu, G., Wang, P., Xia, H., Lin, T., Zhou, P., Hu, W., Meng, X., et al. (2019b). Multimechanism synergistic photodetectors with ultrabroad spectrum response from 375 nm to 10 μm. Adv. Sci. 6, 1901050.

Wang, Y.M., Yu, J.L., Zeng, X.L., Chen, Y.H., Liu, Y., Cheng, S.Y., Lai, Y.F., Yin, C.M., He, K., and Xue, Q.K. (2019c). Temperature and excitation wavelength dependence of circular and linear photogalvanic effect in a three dimensional topological insulator Bi$_2$Se$_3$. J. Phys. Condens. Matter 31, 415702.

Wei, J.X., Xu, C., Dong, B.W., Qiu, C.W., and Lee, C.K. (2021). Mid-infrared semimetal polarization detectors with configurable polarity transition. Nat. Photon. 15, 614.

Wei, J., Li, Y., Wang, L., Liao, W., Dong, B., Xu, C., Zhu, C., Ang, K.W., Qiu, C.W., and Lee, C. (2020). Zero-bias mid-infrared graphene photodetectors with bulk photoresponse and calibration-free polarization detection. Nat. Commun. 11, 6404.

Wu, G., Tian, B., Liu, L., Lv, W., Wu, S., Wang, X., Chen, Y., Li, J., Wang, Z., Wu, S., et al. (2020). Programmable transition metal dichalcogenide homojunctions controlled by nonvolatile ferroelectric domains. Nat. Electron. 3, 43.

Xia, F., Wang, H., Xiao, D., Dubey, M., and Ramasubramaniam, A. (2014). Two-dimensional material nanophotonics. Nat. Photon. 8, 899.

Xu, S., Han, Y., Chen, X., Wu, Z., Wang, L., Han, T., Ye, W., Lu, H., Long, G., Wu, Y., et al. (2015). Van der Waals epitaxial growth of atomically thin Bi$_2$Se$_3$ and thickness-dependent topological phase transition. Nano Lett. 15, 2645.

Yan, Y., Liao, Z.M., Ke, X., Van Tendeloo, G., Wang, Q., Sun, D., Yao, W., Zhou, S., Zhang, L., Wu, H.C., and Yu, D.P. (2014). Topological surface state enhanced photothermoelectric effect in Bi$_2$Se$_3$ nanoribbons. Nano Lett. 14, 4389.

Yang, J., Qin, H., and Zhang, K. (2018). Emerging terahertz photodetectors based on two-dimensional materials. Opt. Commun. 406, 36.

Yang, M., Han, Q., Liu, X., Han, J., Zhao, Y., He, L., Gou, J., Wu, Z., Wang, X., and Wang, J. (2020). Ultrahigh stability 3D TI Bi$_2$Se$_3$/MoO$_3$ thin film heterojunction infrared photodetector at optical communication waveband. Adv. Funct. Mater. 30, 1909659.

Yao, J., Koski, K.J., Luo, W., Cha, J.J., Hu, L., Kong, D., Narasimhan, V.K., Huo, K., and Cui, Y. (2014). Optical transmission enhancement through chemically tuned two-dimensional bismuth chalcogenide nanoplates. Nat. Commun. 5, 5670.

Yu, X., Yu, P., Wu, D., Singh, B., Zeng, Q., Lin, H., Zhou, W., Lin, J., Suenaga, K., Liu, Z., and Wang, Q.J. (2018). Atomically thin noble metal dichalcogenide: a broadband mid-infrared semiconductor. Nat. Commun. 9, 1545.

Zang, C., Qi, X., Ren, L., Hao, G., Liu, Y., Li, J., and Zhong, J. (2014). Photoresponse properties of ultrathin Bi$_2$Se$_3$ nanosheets synthesized by

hydrothermal intercalation and exfoliation route. Appl. Surf. Sci. 316, 341.

Zhang, H., Liu, C.-X., Qi, X.-L., Dai, X., Fang, Z., and Zhang, S.-C. (2009). Topological insulators in Bi$_2$Se$_3$, Bi$_2$Te$_3$ and Sb$_2$Te$_3$ with a single Dirac cone on the surface. Nat. Phys. 5, 438.

Zhang, H., Song, Z., Li, D., Xu, Y., Li, J., Bai, C., and Man, B. (2020). Near-infrared photodetection based on topological insulator P-N heterojunction of SnTe/Bi$_2$Se$_3$. Appl. Surf. Sci. 509, 145290.

Zhang, H., Zhang, X., Liu, C., Lee, S.T., and Jie, J. (2016). High-responsivity, high-detectivity, ultrafast topological insulator Bi$_2$Se$_3$/silicon heterostructure broadband photodetectors. ACS Nano 10, 5113.

Zhang, J., Peng, Z., Soni, A., Zhao, Y., Xiong, Y., Peng, B., Wang, J., Dresselhaus, M.S., and Xiong, Q. (2011). Raman spectroscopy of few-quintuple layer topological insulator Bi$_2$Se$_3$ nanoplatelets. Nano Lett. 11, 2407.

Zhang, T., Levy, N., Ha, J., Kuk, Y., and Stroscio, J.A. (2013). Scanning tunneling microscopy of gate tunable topological insulator Bi$_2$Se$_3$ thin films. Phys. Rev. B 87, 115410.

Zhang, X., and Liu, F. (2021). Prediction of Majorana edge states from magnetized topological surface states. Phys. Rev. B 103, 024405.

Zhang, X., Wang, J., and Zhang, S.-C. (2010). Topological insulators for high-performance terahertz to infrared applications. Phys. Rev. B 82, 245107.

Zhang, Y., Zhang, F., Xu, Y., Huang, W., Wu, L., Dong, Z., Zhang, Y., Dong, B., Zhang, X., and Zhang, H. (2019). Epitaxial growth of topological insulators on semiconductors (Bi$_2$Se$_3$/Te@Se) toward high-performance photodetectors. Small Methods 3, 1900349.

Zheng, W., Xie, T., Zhou, Y., Chen, Y.L., Jiang, W., Zhao, S., Wu, J., Jing, Y., Wu, Y., Chen, G., et al. (2015). Patterning two-dimensional chalcogenide crystals of Bi$_2$Se$_3$ and In$_2$Se$_3$ and efficient photodetectors. Nat. Commun. 6, 6972.

Zhou, J., Lin, J., Huang, X., Zhou, Y., Chen, Y., Xia, J., Wang, H., Xie, Y., Yu, H., Lei, J., et al. (2018). A library of atomically thin metal chalcogenides. Nature 556, 355.

Zhou, S., Wang, R., Han, J., Wang, D., Li, H., Gan, L., and Zhai, T. (2019). Ultrathin non-van der Waals magnetic rhombohedral Cr$_2$S$_3$: space-confined chemical vapor deposition synthesis and Raman scattering investigation. Adv. Funct. Mater. 29, 1805880.

Zhuang, A., Li, J.J., Wang, Y.C., Wen, X., Lin, Y., Xiang, B., Wang, X., and Zeng, J. (2014). Screw-dislocation-driven bidirectional spiral growth of Bi$_2$Se$_3$ nanoplates. Angew. Chem. Int. Ed. Engl. 53, 6425.

Zhuang, H., Yu, J., Chen, L., Gu, P., Chen, Y., Liu, Y., Yin, C., Lai, Y., and Cheng, S. (2021). Giant circular photogalvanic effect of the surface states in an ultra-thin Bi$_2$Se$_3$ nanoplate grown by chemical vapor deposition. J. Appl. Phys. 129, 105303.